TRIBHUVAN UNIVERSITY

INSTITUTE OF ENGINEERING

PULCHOWK CAMPUS

THESIS NO: M-107-MSMDE-2021-2026

Aerodynamic Analysis of Propellers with Dimpled surface and Serrated Trailing-Edge Geometry

BY

Nabin Adhikari (078MSMDE009)

A THESIS

SUBMITTED TO THE DEPARTMENT OF MECHANICAL AND AEROSPACE ENGINEERING

IN PARTIAL FULFILLMENT OF THE REQUIREMENTS FOR THE DEGREE OF MASTER OF SCIENCE IN MECHANICAL SYSTEM DESIGN AND ENGINEERING

DEPARTMENT OF MECHANICAL AND AEROSPACE ENGINEERING

LALITPUR, NEPAL

April 2026

COPYRIGHT

TRIBHUVAN UNIVERSITY
INSTITUTE OF ENGINEERING
PULCHOWK CAMPUS
DEPARTMENT OF MECHANICAL AND AEROSPACE ENGINEERING
PULCHOWK, LALITPUR

APPROVAL PAGE

The undersigned certify that they have read, and recommended to the Institute of Engineering for acceptance, a thesis entitled, " **Aerodynamic Analysis of Propellers with Dimpled surface and Serrated Trailing-Edge Geometry**" submitted by Mr. Nabin Adhikari (078/MSMDE/009) in partial fulfillment of the requirement for the degree of Master of Science in Mechanical System Design and Engineering.

.....

Supervisor,
Prof. Dr. Rajendra Shrestha,
Department of Mechanical and Aerospace Engineering,
Institute of Engineering, Pulchowk Campus

.....

External Examiner,
Er. Bikki Chhantyal,
Institute of Engineering, Thapathali Campus

Tribhuvan University
Institute of Engineering
Department of Mechanical and Aerospace Engineering
Pulchowk Campus

.....

Committee Chairperson, Asst. Prof. Sudip Bhattarai, PHD,
Head of the Department,
Department of Mechanical and Aerospace Engineering,
Institute of Engineering, Pulchowk Campus

Date: 2026/04/27

iii

ABSTRACT

The rapid growth of small unmanned aerial vehicles (UAVs) caused the surge in demand for propeller designs that can maintain high aerodynamic efficiency operating in low-to-moderate Reynolds number, where laminar flow separation and unsteady wake structures significantly degrade performance of the propeller. This study investigates the aerodynamic behavior of small-scale UAV propellers incorporating bio-inspired passive surface modifications, specifically circular surface dimples and serrated trailing-edge geometries.

A baseline propeller based on the NACA 4412 airfoil was designed using Blade Element Momentum Theory and subsequently modified with dimples on the surface, serrations, and combined dimpled–serrated configurations. Aerodynamic performance was evaluated through a combination of computational fluid dynamics (CFD) simulations in ANSYS Fluent and experimental static thrust testing of resin-printed propellers over a range of Revolutions Per Minute (RPMs).

Experimental results showed that the dimpled propeller consistently outperforms the baseline propeller, achieving approximately 13-15% higher maximum thrust at comparable RPMs which could be the result of delayed boundary-layer separation and enhanced pressure recovery. The propeller with serrations on trailing edge showed only marginal thrust improvement, even performing worse at lower RPM, while the combined dimpled–serrated configuration provided a sweet spot of performance, indicating a balanced aerodynamic compromise compared to its counterpart. Although CFD predictions capture the ideal performance trends and often yield higher values, quantitative discrepancies arise due to idealized numerical assumptions, unmodeled surface roughness, minor aeroelastic deformations, and inherent limitations of the Transition SST turbulence model when compared with experimental conditions.

Overall, the study confirms that surface dimples significantly enhance low-Reynolds-number propeller performance, while combined dimpled–serrated geometries offer a promising design pathway for UAV applications requiring a trade-off between thrust performance and potential acoustic mitigation.

Keywords: UAV propellers, passive flow control, surface dimples, serrated trailing edge, low Reynolds number aerodynamics, CFD, experimental validation.

ACKNOWLEDGEMENT

First and foremost, I would express my sincere gratitude to my respected thesis supervisor Prof. Dr. Rajendra Shrestha for his exceptional constant guidance, valuable advice, patience, knowledge, continuous support and willingness to allow me to pursue the study on aerodynamic analysis of propellers with dimpled surface and serrated trailing-edge geometry, which made this research work possible and successful. His thoughtful guidance and valuable suggestions helped me work harder and improve at every stage of my research work.

I would like to acknowledge all the faculty members of Department of Mechanical and Aerospace Engineering for the knowledge, support and fundamental concepts they shared with me during my study at IOE, Pulchowk Campus. I would like to thank Asst. Prof. Kamal Darlami for his invaluable guidance, encouragement and support during the completion of this thesis work.

I am equally grateful to my friends MSMDE/078 batch for their cooperation and insightful suggestions. I would like to express my sincere appreciation to my dear friend, Er. Anuska Gautam, for her invaluable support, guidance, and thoughtful suggestions throughout my study. I am also deeply grateful to Er. Shishir Gyawali for his intellectual companionship; his insightful discussions and constructive input greatly contributed to the completion of this work. My sincere thanks also go to everyone who provided valuable support, critical comments, suggestions and advice on different stages of my research work.

Last but not the least, I would like to start off by thanking my parents, including my sister, for their persuasion and continuous support throughout my academic perseverance. They were always there cheering me up and stood by me through good and bad times, which motivated me to overcome the difficulties and led to this stage of my thesis.

Nabin Adhikari

078/MSMDE/009

April 2026

Table of Contents

List of Figures

List of Symbols

T	Thrust
dT	Thrust from small blade section
r	Local radius
dr	Small radial thickness
Δp	Pressure jump across disk
B	Number of blades
R	Propeller radius
D	Propeller diameter
ϕ	Inflow Angle
V	Free stream velocity (aircraft speed)
v_i	Induced Velocity
β	Blade pitch angle
ϕ	Inflow angle
α	Airfoil angle of attack
ρ	Air density
V_r	Relative Velocity
c	blade chord
C_L	Lift coefficient
C_D	Drag coeffiecient
dr	Radial width
NACA	National Advisory Committee for Aeronautics
Mpa	Mega Pascal
HD	Shore D
g	gram
V	Voltage
A	Current
DC	Direct Current

CHAPTER ONE:
INTRODUCTION

1.1 Outline of the study

The main goal of this thesis is to conduct thorough research on the aerodynamic behavior of dimpled serrated propeller, or those with a dimpled surface and serrated trailing edge. This study attempts to produce the result that investigates the real-life scenario application of dimpled serrated propellers. The outcomes are presented in such a manner that it will reveal the aerodynamic behavior such propeller compared to conventional commercially available propellers. Commercially available ANSYS Fluent is used for CFD analysis has been used to create a sequence of models for this assignment with consideration of proper meshing parameters. These models will then be utilized to provide qualitative foundation for the problem results. Firstly, the model of base propeller with NACA 4412 airfoil profile will be analyzed. Secondly, the model of identical airfoil geometry with dimpled surface, serrated edge and combination of both with various parameters will be analyzed. The results, as well as their impact, are described in this dissertation, which is a complete study aimed at evaluating the impacts on the aerodynamic behavior of dimpled and serrated trailing edge on the propeller.

1.2 Background

Propeller is a rotating device with blades that are used in diverse sectors from aerospace, marine to automotive. For the successful, effective and safe operation of equipment in these sectors proper functioning of propellers plays a crucial role. Propeller's aerodynamic behavior combined with acoustic behavior is one of the key problems in fluid dynamics. Propeller itself is just a component comprising of blades, when it's attached to a rotating component, its application and behavior is determined. The blades are shaped so that their rotational motion through the fluid causes a pressure difference between the two surfaces of the blade by Bernoulli's principle which exerts force on the fluid. Many factors, including the number of blades, blade form, blade twist, blade angle, and use, can be used to categorize propellers.

Small unmanned aerial vehicles (UAVs) and multirotor drones are increasingly used in surveillance, delivery, and environmental monitoring, where aerodynamic efficiency and acoustic stealth are critical. Propeller-generated drag and noise-dominated by boundary-layer separation, tip vortices, and trailing-edge vortex shedding limit areas of application and effectiveness on certain scenarios. Noise characteristics of multirotor drones and UAV's have

been analyzed, and it has been found that noise generated by the propellers, in overall, is much greater than the noise generated by the motors itself (Gu, et al. 2024).

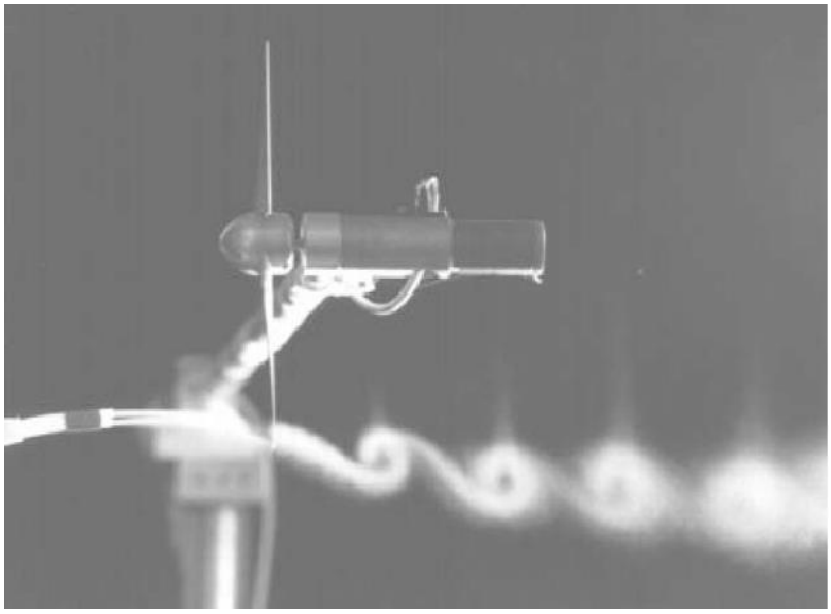

Figure 1.1: Flow visualization of a tip vortices of a two bladed rotor (Vermeer, Sorensen and Crespo 2003)

Dimpled surfaces are inspired by the aerodynamic properties of golf balls, which utilize surface indentations to create a thin, turbulent boundary layer that "clings" to the surface longer (Bearman and Harvey 1993). This indentation transitions the flow to a turbulent state earlier, energizing it to better combat the adverse pressure gradient and pushing the point of separation further downstream. Numerical and experimental investigations demonstrate that dimples whether inward or outward and in various geometries such as spherical, hexagonal, or semi-cylindrical can produce a substantial boost in the lift-to-drag (L/D) ratio. This performance enhancement is particularly significant at high angles of attack, where dimples create vortices and swirl that effectively reduce the size of the wake zone.

Reducing trailing-edge noise, which is one of the main sources of propeller broadband noise, is crucial for urban air mobility and operation in addition to performance optimization. Trailing-edge noise is produced when the strong geometric discontinuity of the blade's edge scatters turbulent fluctuations within the boundary layer in the form of sound. Inspired by the distinctive wing structure of birds, especially owls, serrated trailing-edge designs are known to reduce the propeller noise by changing the scattering behavior in turn altering the efficiency of turbulent pressure fluctuations.

A thorough study of these passive control techniques is crucial for the development of next generation of silent, efficient, and high-performing aerial vehicles. By balancing the aerodynamic benefits of dimpled surfaces with the aero-acoustic advantages of advanced serrated trailing edges, designers can achieve multi-functional surfaces tailored for optimal operation in complex flow regimes.

To examine the aerodynamic behavior of low Reynolds-number propellers, which are frequently used for small-scale UAVs and drones, this study focuses on a combined passive flow-control technique, employing surface dimples (circular) and serrated trailing-edge geometries. The work involves analytical modeling, computational fluid dynamics (CFD) simulation, and experimental comparison with propellers that are available commercially.

1.3 Problem Statement

Aerodynamic drag, boundary-layer separation, tip vortices, and trailing-edge vortex shedding substantially reduce propeller efficiency and generate broadband noise in low-to-moderate Reynolds number operating conditions, where small unmanned aerial vehicles (UAVs) and drones generally operate.

For many UAV applications, these effects are problematic since they reduce flight duration and increase noise detectability. Commercial UAV propellers currently available on the market are primarily designed to maximize thrust and manufacturing efficiency, with minimal incorporation of passive flow-control methods meant to reduce drag and noise levels at the same time.

The combined effectiveness resulting from surface dimples and trailing-edge serrations on small-scale spinning UAV propellers is still insufficiently understood, even though each has individually demonstrated aerodynamic and aero-acoustic benefits in airfoil designs and large-scale applications. Validated theoretical models and numerical frameworks that provide optimal dimple shape and serration parameters under practical UAV operation conditions are missing. To fill this gap and develop meaningful design guidelines for more effective and silent UAV propellers, a systematic investigation combining propeller theory, computational fluid dynamics, and experimental analysis is essential.

1.4 Objectives of the Research

1.4.1 Main Objective

- The aerodynamic performance and behavior of propellers crucially depend on the surface geometry. This study's primary goal is to characterize the aerodynamic behavior of propellers with surface dimples and serrated trailing edges

1.4.2 Specific Objectives

- To analytically characterize and model propellers in CAD
- To design and evaluate circular dimple shapes suitable for propeller blades with low Reynolds numbers, along with their influence on boundary-layer behavior and drag reduction
- To design serrated trailing-edge shapes and assess their impact on thrust output
- To conduct CFD simulations in ANSYS Fluent to assess variations in thrust, and flow structures induced by dimpled and serrated modifications
- To validate numerical results through static thrust experimental setup using baseline and modified propeller designs

This study is based on the hypothesis that surface dimples enhance aerodynamic performance by delaying boundary-layer separation in low-Reynolds-number propellers, while trailing-edge serrations modify wake dynamics and reduce vortex coherence. Furthermore, it is hypothesized that a combined dimpled–serrated configuration provides an optimal balance between thrust generation and aerodynamic losses for small UAV propellers.

1.5 Scope and Limitation of the study

Commercial propellers are manufactured using composite materials and carbon fiber due to which they can run at higher rpm and have much smoother surface. Since this thesis encompasses the effect of dimpled surface and serrated trailing edge geometry on propellers that are 3D printed with consideration on material strength, and running rpm, it provides a meaningful estimation of the aerodynamic behavior of such propellers.

The research is limited to single dimple and serrated trailing edge geometry, which might not be favorable for wide range of geometrical modifications that are possible and can change the

aerodynamic and aero-acoustic behavior completely. Some of other limitations are listed below:

- Propellers during their operation generate torque inherently, but our study primarily focuses on the thrust and efficiency of propellers at certain rpm
- Only aerodynamic behavior of the propellers is evaluated not the aeroacoustics behavior

Apart from these, study is restricted to the limited range of parameters, which may not take account to actual problems in field.

CHAPTER TWO:
LITERATURE REVIEW

This section includes a brief review of previous studies and literature that have been conducted and published required to understand the basic foothold for the study. The literature review focuses on recent contributions related to the study of behavior of passive surface modifications on propellers. Forepart of this section includes the basic definitions and theories regarding the study whereas the subsequent part includes the review of previous research studies.

2.1 Introduction

The design and optimization of small-scale propellers have gained significant prominence with the rapid proliferation of Unmanned Aerial Vehicles (UAVs). Propellers operate in low-to-moderate Reynolds numbers at these scales, where performance is often compromised by significant trailing-edge noise and laminar flow separation. With the goal to improve the aerodynamic efficiency and reduce acoustic noise, researchers have turned to bio-inspired passive surface modification strategies.

Among these methods, dimpled surfaces that resemble a golf ball's topology are utilized to change the boundary layer from laminar to turbulent, delaying flow separation and lowering pressure drag. To substantially reduce broadband noise, turbulent eddies are separated as they shed from the blade using serrated trailing edges, which are modeled based upon the quiet flight of owls.

However, there are significant aerodynamic tradeoffs involved in putting such modifications into practice. Dimples on the surface can increase skin friction in high-speed applications, but they may decrease drag at high angles of attack. Similarly, serrations can lessen noise but may also result in a smaller effective lifting surface, which could lower thrust. Designing next-generation, high-performance, ultra-quiet propulsion systems requires an understanding of the combined impact of these improvements on both aerodynamic efficiency and aeroacoustic behavior. The existing experimental results and mathematical models regulating these passive flow control techniques are examined in this review.

2.2 Propeller Design

The optimization of the blade's radial sections to obtain a specific thrust-to-power ratio is the foundation of conventional propeller design. Each blade segment is regarded as a separate

airfoil that must operate in a complicated, rotating flow environment while balancing the local lift and drag forces. When constructing a propeller, Blade Element Momentum Theory (BEMT) must be considered.

To take into consideration for the increasing tangential velocity from the root to the tip, the geometric definition typically relies on the chord distribution and the pitch (twist) angle along the radius. Engineers maintain a consistent pressure distribution by keeping a fixed angle of attack across the blade. Although effective, these conventional designs are limited by the physical characteristics of the chosen airfoil; at lower speeds, they often suffer from laminar separation bubbles and high-frequency vortex shedding at the trailing edge. For evaluating any subsequent surface or edge alterations, this baseline performance serves as the control group.

2.2.1 Blade Element Momentum Theory Fundamentals

Blade element momentum theory is a combined theory that incorporates blade element theory and momentum theory. It is used to calculate the local forces on a propeller or wind-turbine blade. Figure 2.1 shows a stream tube where free stream is flowing and passing over an actuator disk. The annular ring shows the small area at specific section of the radius of actuator disk.

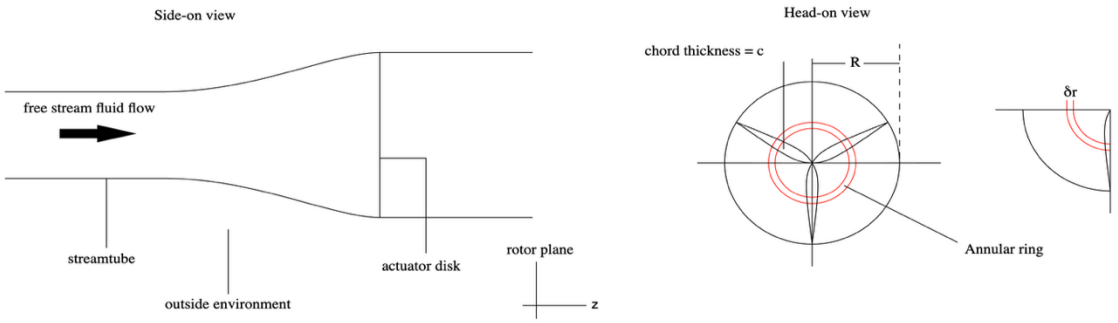

Figure 2.1: Axial free stream fluid setup (Jenkins 2001)

Blade element momentum theory deals with the flow of air, it overlooks few other key factors like torque. Blade element theory deals primarily with the forces on the propeller. Blade element theory considers the propeller blade made up of numbers of small elements and calculating forces on each element.

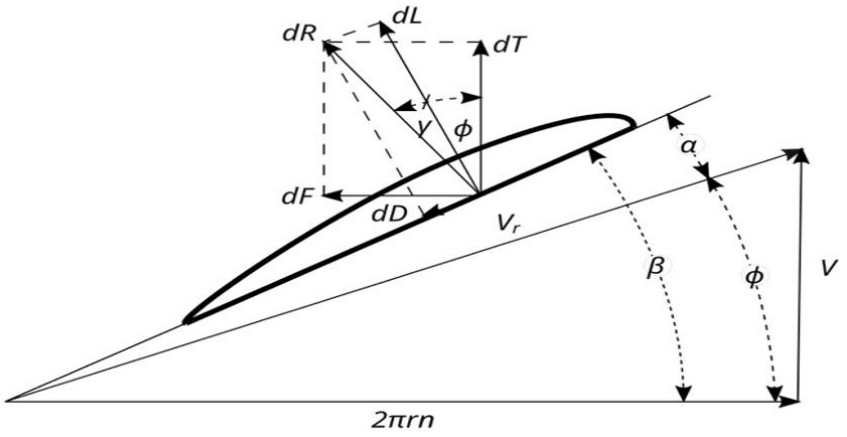

Figure 2.2: Components acting on a propeller cross section

Considering uniform loading across the active annulus $[r_0, r_1]$ the thrust can be calculated for the section using

$$dT = \Delta p \cdot 2\pi r\, dr \Rightarrow \frac{dT}{dr} = 2\pi r \Delta p \tag{1}$$

Total thrust over the annulus is calculated using Equation (2) and it can be written as Equation (3) for pressure jump.

$$T = \Delta p \cdot \pi(r_1^2 - r_0^2) \tag{2}$$

$$\Delta p = \frac{T}{\pi(r_1^2 - r_0^2)} \tag{3}$$

This results in the thrust distribution which is represented by Equation (4)

$$\frac{dT}{dr} = \frac{2T}{(r_1^2 - r_0^2)}\, r \tag{4}$$

This shows thrust is increasing linearly with radius which makes sense since the outer sections of the propeller move faster and sweep more area. The multiplier part of Equation 4 can be written as Equation (5).

$$k = \frac{2T}{(r_1^2 - r_0^2)} \tag{5}$$

Where *k* is considered as the strength of thrust distribution along the blade.

In real cases the propellers do not produce ideal calculated thrust at the root/base and tips. This happens because air slips around the tips causing tip vortices which cause losses and are one of the key factors behind the noise generated by the propeller. Similarly, near the hub of the propeller losses occur due to it moving slower compared to other sections of the blade and the

hub geometry produces little to no lift. To correct this, we use Prandtl loss factors which are represented by Equation (6), (7), (8), (9) and (10) respectively.

Tip Loss Factor:

$$f_{\text{tip}} = \frac{B}{2}\frac{(R-r)}{r\sin\phi} \tag{6}$$

Tip Loss:

$$F_{\text{tip}} = \frac{2}{\pi}cos^{-1}\left(e^{-f_{\text{tip}}}\right) \tag{7}$$

Root Loss Factor:

$$f_{\text{root}} = \frac{B}{2}\frac{(r-r_h)}{r\sin\phi} \tag{8}$$

Root Loss:

$$F_{\text{root}} = \frac{2}{\pi}\cos^{-1}(e^{-f_{\text{root}}}) \tag{9}$$

Combined Loss

$$F = F_{tip}F_{root} \tag{10}$$

At the radius r, the blade element sees two velocity components which we can see in Figure 4. The resultant velocity V_r can be calculated using Equation (11)

$$V_r = \sqrt{V^2 + Vt^2} \tag{11}$$

Where V is the axial velocity of air moving through the propeller and V_t is the tangential velocity both of which can be calculated with the help of Equation (12) and (13)

$$V = V_\infty + v_i \tag{12}$$

$$V_t = \Omega * r \tag{13}$$

In hover condition, with loss factor considered the induced velocity v_i can be calculated using Equation (14)

$$v_i = \sqrt{\frac{(dT/dr)}{4\pi\rho rF}} \tag{14}$$

The inflow angle determines the angle of incoming air and is calculated using Equation (15)

$$\phi = \tan^{-1}\left(\frac{V}{V_t}\right) \tag{15}$$

In hover static condition the free stream velocity V_∞ is considered as 0 and inflow angle can be calculated using just the induced velocity. Each section of the blade is at a specific angle of attack. The relation between the angle of attack, blade pitch angle and inflow angle is represented by the Equation (16)

$$\beta = \phi + \alpha \tag{16}$$

Each element on the propeller blade acts like an airfoil and lift and drag at each section can be calculated using Equation (17) and (18)

$$dL = \frac{1}{2}\rho {V_r}^2 c C_L dr \tag{17}$$

$$dD = \frac{1}{2}\rho {V_r}^2 c C_D dr \tag{18}$$

Lift and Drag aren't aligned in the propeller axis, resolving them into thrust direction results in the contribution to the thrust which can be calculated using the Equation (19)

$$dT = B(dLcos\phi - dDsin\phi) \tag{19}$$

In similar way we can calculate the torque generated by the propeller using Equation (20)

$$dQ = Br(dLcos\phi + dDsin\phi) \tag{20}$$

The core idea behind momentum theory is that blade element thrust is equal to the momentum thrust generated by the change in momentum of the airflow. The change in momentum of the airflow can be written with the help of Equation (21)

$$dT = 4\pi r\rho V v_i dr \tag{21}$$

Equating Equation (19) and Equation (21) we can then solve for induced velocity and blade geometry. Equation (22) helps us determine the blade geometry at different sections.

$$B(dLcos\phi - dDsin\phi) = 4\pi r\rho V v_i dr \tag{22}$$

For optimal efficiency the chord varies along the radius of the propeller, and it can be derived with the help of Equation (23).

$$c = \frac{(dT/dr)}{\frac{1}{2}\rho\, B\, W^2 (dLcos\phi - dDsin\phi)} \tag{23}$$

We can check the Reynold's Number at each section using the chord and resultant velocity. The Reynold's number at each section are calculated with the help of Equation (24)

$$Re = \frac{\rho V_r c}{\mu} \tag{24}$$

To maintain the optimal angle of attach the propeller blades get twisted as it moves from hub to the tip. The blade pitch angle at each section can be determined by Equation 10. The local pitch at radius r can be calculated using the blade pitch angle by

$$P = 2\pi r \tan\beta \tag{25}$$

Using iterative approach at different radial distances we can calculate the pitch angle, chord length, Reynold's number. Using these iterated values, we can then create a geometric model of the propeller in a CAD software.

2.3 Passive Surface Modification

Passive surface modifications represent a biomimetic approach to fluid dynamic control, where fixed geometric alterations are used to manipulate the boundary layer without external power input (Farid and Chamorro 2026). These techniques are primarily designed to delay flow separation, reduce skin friction, or suppress aeroacoustic noise. On propellers and wind turbines, leading-edge protuberances inspired by the tubercles on humpback whale flippers are used to generate streamwise vortices (Li, Liu and Li 2021).

By re-energizing the boundary layer, these vortices delay the onset of stalling and enable the component to maintain lift at higher angles of attack. Riblets, which are tiny V-shaped grooves, are used on the fuselage and wing surfaces of aircraft with high Reynolds numbers. By interacting with near-wall turbulent structures, these structures can reduce turbulent skin friction by as much as 8%. Serrated trailing edges are becoming increasingly frequent on wind turbine blades and aircraft engine chevrons for aeroacoustic suppression. By disrupting the span-wise coherence of turbulent eddies, these serrations allow noise to shift to higher, less audible frequencies (Zhang, et al. 2025).

In order to induce local turbulence and keep the flow attached over the blade's suction side, dimpled surfaces are also studied for low-speed airfoils (Ali, et al. n.d.). Though these changes have several advantages, they must be carefully adjusted to the local Reynolds number to avoid parasitic drag penalties.

2.3.1 Tubercles

The humpback whale's pectoral flippers serve as the model for tubercles, a bio-inspired protrusion. These tubercles generate counter-rotating chord-wise vortices which act as passive flow control mechanisms in aerodynamic applications. By moving high-momentum fluid from the free-stream toward the blade surface, these vortices reenergize the boundary layer. Compared to a smooth-edged equivalent, this mechanism effectively delays flow separation, enabling the propeller or airfoil to maintain lift at considerably higher angles of attack.

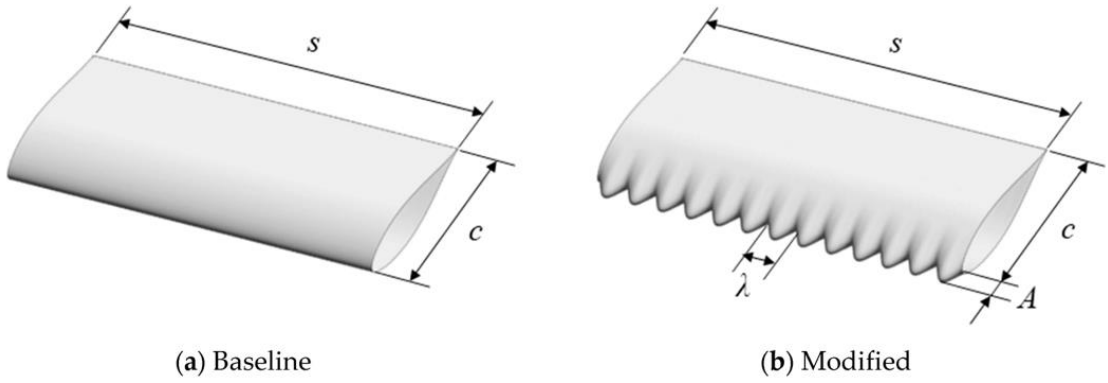

Figure 2.3: Leading edge tubercles on an airfoil (D. Wang, et al. 2024)

As an outcome, abrupt stall characteristics can be suppressed by tubercles, changing a sudden loss of lift into a more gradual and controllable transition. Their capacity to improve agility and maintain performance in highly turbulent or unstable flow conditions makes them indispensable for specialized propellers and wind turbine blades, even if they could cause a slight drag penalty at low angles of attack. A sine or cosine curve with a particular period, amplitude, and wavelength is typically followed by protrusions.

2.3.2 Serrations

To reduce aeroacoustic noise, serrations, tooth-like geometric modifications are mainly applied to the trailing edges (TE) of propellers and airfoils. These structures, which are modeled after the wings of owls, cause turbulent eddies to lose their span-wise coherence when they cross the trailing edge.

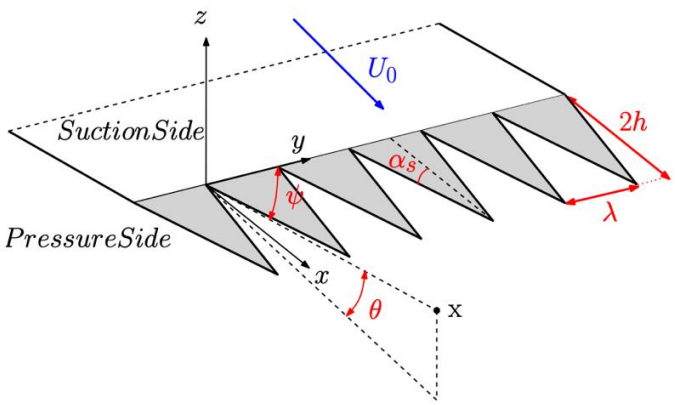

Figure 2.4: Sketch of trailing edge serrations (Gruber 2012)

Serrations create destructive interference of sound waves by dividing large-scale vortices into smaller, less energetic structures, so "smearing" the acoustic signature throughout a wider frequency range (Sustainability Directory 2025). Trailing-edge serrations are an essential component of stealthy UAV design and urban air mobility, even though they are primarily employed for noise reduction, they can also affect lift characteristics and wake formation.

2.3.3 Dimples

Inspired by golf ball aerodynamics, dimples are a passive surface modification intended for controlling the boundary layer in low Reynolds number regimes (Ali, et al. n.d.). When applied to the suction side of a propeller or airfoil, dimples act as turbulators that trigger a controlled transition from laminar to turbulent flow (S and S 2017).

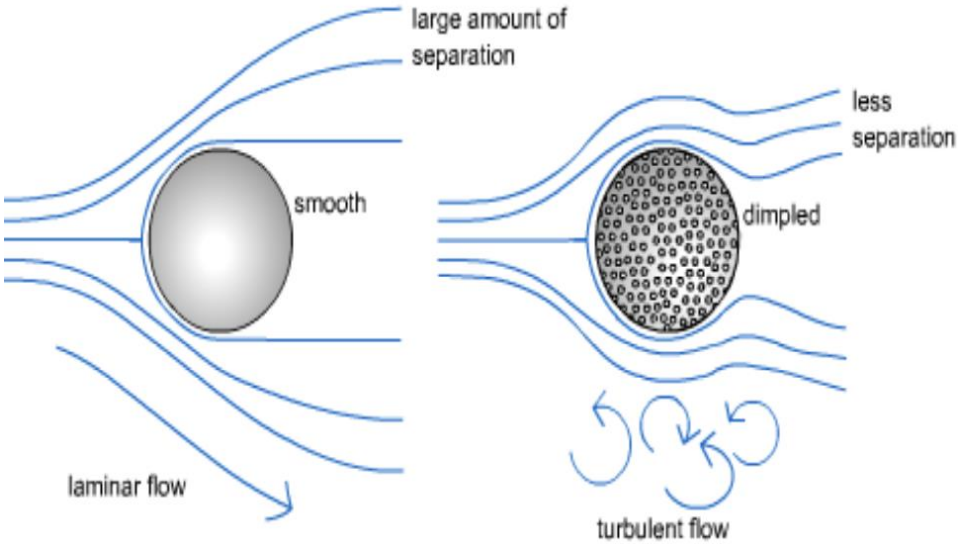

Figure 2.5: Flow over a golf ball with and without dimples (S and S 2017)

This turbulent boundary layer is more energetic and better able to resist adverse pressure gradients, which delays flow separation and reduces the size of the wake. For small-scale propellers, this modification helps eliminate laminar separation bubbles, effectively reducing pressure drag and maintaining thrust efficiency at high angles of attack.

2.4 Passive surface modifications on propellers

Several research have looked at how serrated edge geometry affect noise production using numerical simulations with computational fluid dynamics (CFD). For instance, asymptotic theory by (Howe 1991) shows that significant reductions in trailing edge noise are possible when the edge is serrated. It was in accordance with the limited experimental observation conducted at the time. Moreover, CFD simulations done by (Kim and Jeon 2019) demonstrated that altering the propeller design can greatly lessen the intensity of tip vortices, which in turn reduces noise output.

In numerous research, experimental testing has also been utilized to assess how well-up-to-date propeller designs reduce noise. For instance, (Kim, et al. 2017) experimental testing revealed that a modified toroidal propeller design produced less noise than a standard propeller design. (Moreau and Doolan 2013) conducted an experimental investigation exploring the noise reduction potential of sawtooth trailing edge serrations on a flat plate at low-to-moderate Reynolds number ($1.6 \times 10^5 < Re < 4.2 \times 10^5$). Their results demonstrate that a trailing edge serration achieved reduction of noise by up to 13 dB in narrowband noise levels and this is mainly due to attenuation of vortex shedding at the trailing edge. Contrary to the theory by (Howe 1991) wide serrations with larger wavelength to amplitude ratio, λ/h, were found to outperform narrow ones by achieving higher attenuation levels and no noise increase in the mid frequency region.

(Candeloro, Ragni and Pagliaroli 2024)demonstrated how serrated drone blades can mitigate broadband noise components while simultaneously reducing tonal noise components. Their paper conducted an experimental study involving he design, manufacture, and testing of 23 propellers was performed to establish a relationship between serration geometry and noise mitigation. Acoustic characterization during hovering was carried out at a constant rotational speed of RPM using near-field microphone measurements. The primary drawback that they saw in their study was the reduction in thrust generated by the propeller.

(Abdullah and Dol 2020) looked into the aerodynamic performance of dimpled airfoil for drones and UAVs propellers. Their aim was to check if dimples will improve the efficiency of

the structure by increasing lift to drag ratio and stall angle or decreasing drag force on the airfoil. In their Ansys Fluent simulations they found the dimpled airfoil had a better L/D ratio compared to a traditional one. Moreover, the efficiency of the dimpled airfoil increased by around 39.9% at an angle of attack of 12°.

Study conducted by (Gattere, Chiarini and Quadrio 2022) offers insightful information on how dimples can be used to reduce skin-friction drag. It is perhaps the most essential manifestation of the dissipative nature of turbulence and accounts for the total drag in the case of planar walls (as in a channel flow or a zero-incidence flat plate boundary layer). While they were unable to answer the still-standing question on whether dimples are a suitable technique to reduce turbulent skin-friction drag compared to riblets, they were able to provide up-to-date description of what we know and what we don't about potential impact of dimples on drag reduction.

Using direct numerical simulations (Sudarsana, Singh and Sareen 2025) investigated the effect of surface dimples on the unsteady aerodynamics of NACA0012 airfoil. At a constant angle of attack $\alpha = 5^{\circ}$, using direct numerical simulations at Reynolds numbers $Re_c = 5300$ and $Re_c = 10{,}000$, they found mean lift and drag coefficients remained largely unchanged, significant differences were observed in the unsteady force response. Their study suggested that dimples not only stabilize the dominant unsteady modes but also suppress wake irregularities, delaying the onset of vortex breakdown.

Inline arrangement of dimples on airfoil has been found to reduce the noise generated by them significantly. The position of dimples on the surface is crucial in achieving the required result. In a study conducted by (Kumar, et al. 2024) dimples positioned at $1/3^{rd}$ of the chord from the leading edge provided significant noise reductions of about 6-8 dB, however, when the position was changed to $1/5^{th}$ of the chord length from the leading edge the degree of noise reduction reduced significantly. Along, with drag reduction possibility, the dimples can also contribute to the reduction of broadband noise generated by propellers. (Jorgensen 1994)

In the study conducted by (Fikadea, et al. 2020) on wind turbine blades with dimples added to the surface, they found that maximum aerodynamics performance occurred at an angle of attack of 12° and flow separation started to occur at angles higher than 15°. Particularly the inward dimples on the suction side showed a noticeable enhancement compared to one with outward or no dimples at all. Their experimental result showed dimples increased aerodynamic performance by delaying the flow separation even at higher angle of attack.

CHAPTER THREE:
METHODOLOGY

3.1 Conceptual Framework

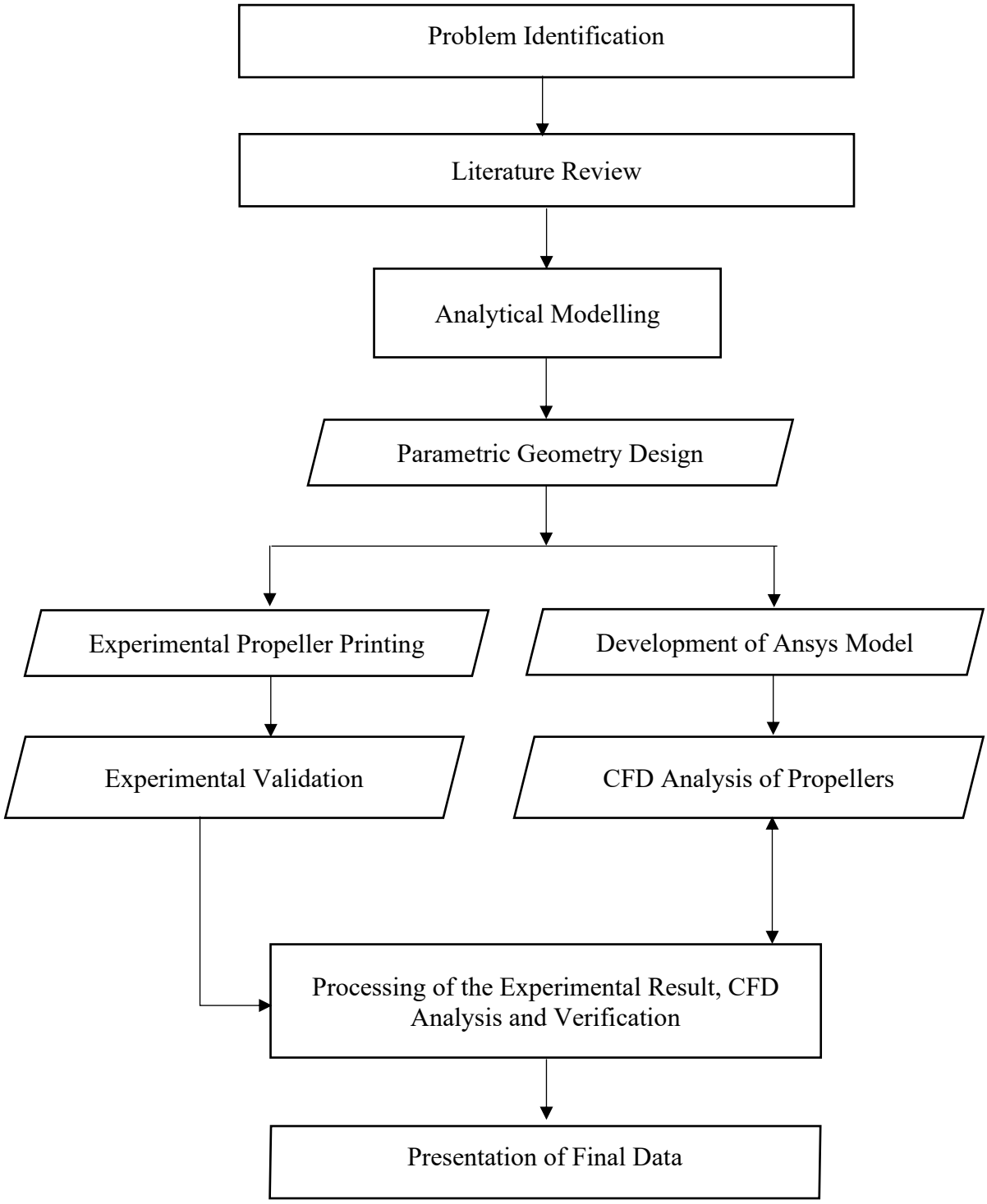

Figure 3.1: Flowchart of Research Methodology

The research will be conducted in 7 phases:

1. Problem Identification
2. Literature Review
3. Analytical Modeling
4. Parametric Geometry Design
5. Computational Analysis
6. Experimental Validation
7. Results and Discussion

3.2 Problem Identification

Propellers are widely used in various engineering systems such as unmanned aerial vehicles (UAVs), marine propulsion systems, wind turbines, and small aircraft. The aerodynamic performance of a propeller is primarily determined by the geometry of its blades, including parameters such as chord distribution, pitch angle, airfoil shape, and surface characteristics. Conventional trailing edges and smooth blade surfaces are common in traditional propeller designs. Despite substantial research and optimization, flow separation, tip vortices, and turbulent wake production continue to result in aerodynamic losses in these designs.

Enhancing thrust generation while simultaneously reducing aerodynamic drag, noise, and energy losses is a significant challenge in propeller aerodynamics. The airflow over the propeller blade may change from laminar to turbulent flow at higher rotational speeds or under varying operating conditions, increasing drag and decreasing efficiency. Furthermore, vortex generation and energy dissipation in the wake region are facilitated by flow separation close to the trailing edge and blade tips. Propeller performance and overall efficiency are restricted by these aerodynamic phenomena.

Biomimetic and textured surface geometries can affect boundary layer behavior and improve aerodynamic performance, as demonstrated by recent research on aerodynamic surface modification. It has been shown that surface alterations like dimples, which are modeled after the surface geometry of golf balls, lower pressure drag by facilitating controlled turbulence in the boundary layer. Similarly, by changing the wake pattern behind aerodynamic surfaces, serrated trailing edges, inspired by the wing structure of owls and other birds, have shown promise in lowering noise and weakening vortex shedding.

Although dimpled surfaces and serrated trailing edges have their own benefits, their combined use in propeller blade design has not been well studied. The majority of current propeller research focuses on either traditional smooth blade designs or modifications like winglets, tubercles, and blade twist optimization. Particularly in the context of small-scale propellers employed in UAVs and low Reynolds number operating conditions, the aerodynamic interaction between dimple-induced boundary layer management and serrated trailing-edge vortex modification remains insufficiently understood.

Moreover, the aerodynamic behavior of small propellers is quite different from compared to larger aircraft propellers since they usually operate in low Reynolds number regimes. Under these circumstances, flow separation happens more easily, and aerodynamic performance can be greatly affected by small geometric changes. Therefore, increasing propeller efficiency in such applications requires an understanding of how dimpled serrated designs affect lift, drag, thrust generation, and wake characteristics.

Thus, the purpose of this work is to use computational analysis and analytical modeling to examine the aerodynamic performance of propellers with dimpled serrated shape. Understanding how these surface alterations affect aerodynamic forces, flow separation, vortex formation, and overall propeller efficiency will be the primary objective of the study. The outcomes of this research should help develop better propeller design techniques for small-scale propulsion systems and provide insight into potential advantages associated with specific surface geometries in aerodynamic applications.

3.3 Literature Review

Studies on dimples and serrations have demonstrated that they reduce drag and dampen noise on large sized rotors and fixed wings. Nevertheless, little study has been done on small-scale rotating UAV propellers under practical operating circumstances. With the objective to support design parameters, turbulence models, CFD methodologies, and experimental validation techniques, pertinent papers are evaluated. Resources related to the design and performance parameters will be collected from appropriate sources and carefully reviewed. Several works on trailing edge vortices, fluid flow, acoustic behavior, and propeller design parameters are cited. This will provide all the groundwork and information required to complete the research project successfully. As of today, several studies on propellers, tip vortices, noise characteristics, and CFD modeling have already been examined; additional studies will be conducted throughout this research work.

3.4 Analytical Modelling

From the data sources that are available, baseline propellers are modeled. Chord, twist, angle of attack, Reynolds number distribution, and loading along the span are all evaluated using Blade Element Momentum Theory (BEMT). Without sacrificing thrust requirements, this offers reference operating regions and directs the arrangement of dimples and serrations.

For the design of propellers NACA 4412 airfoil was selected. Several research has already been conducted with airfoils like NACA 0012, NACA 2412, NACA 4412 and so on. The selection of this airfoil was done due the manufacturing and 3D printing limitation that happens with thin and minute structures. NACA 4412 airfoil has much a lower thickness to chord ratio compared to NACA 4418 and other similar profiles, which might cause the physical blade to be thinner and more flexible, inturn inducing flutter and vibration at higher RPM's. The design parameters for the propeller are listed below:

Table 3.1 Design Parameters for the Propeller

Parameter	Symbol	Value
Airfoil	-	NACA 4412
Angle of Attack	α	6.5°
Thrust	T	3N
RPM	RPM	10000
Diameter	D	8 inch
Radius	R	4 inch
Hub Radius	-	0.2R

The angle of attack was chosen to be 6.5 degrees. This value was chosen because several literatures were reviewed and found that the angle of attack between the range of 4 - 7 degrees resulted in optimal results. The value for coefficient of lift and drag at the angle of attack of 6.5 and Reynolds number 50000 was taken from airfoil tools site. The calculated value of the Reynold's number at 75% of radius was found to be approximately 23000. The thrust, pitch angle, and chord length all were calculated at different sections starting from 20% of radius to 95% of radius of propeller. The diameter of the propeller was chosen to be 8 inch and the RPM taken for the design consideration was 10000 RPM.

3.5 Parametric Geometry Design

3D model for both conventional propeller and serrated dimpled propeller will be generated using commercially available CAD software i.e., SolidWorks, CATIA. The models will then be used in CFD software (ANSYS Fluent) alongside getting 3D printed for experimental testing.

3.5.1 Base Propeller Geometry

The base propeller geometry is modelled in SolidWorks with the calculated chord length at multiple blade sections. Since the geometry is quite small and the features are also small several planes were created with spacing between them increasing at with the blade radius. This can be seen in Figure 3.2. The shaft hole diameter was set to 7mm to match the motor shaft.

The twisting of the blade as the radius increases can be seen properly in Figure 3.3. As the radius is increasing so is the chord length, but as we approach the tip of the propeller blade the chord length decreases significantly. The geometry is modeled using the loft functionality in SolidWorks connecting airfoil curves at different planes which represents the sections of the propeller.

Figure 3.2: Base Propeller Geometry

Figure 3.3 Front view of the propeller

3.5.2 Serrated Propeller Geometry

Trailing-edge serrations are defined by amplitude, wavelength, and spanwise distribution. All modified geometries are CAD-modeled with manufacturability constraints. To calculate the height, wavelength and serration angle we start with the calculating the boundary layer thickness. Reynolds number was calculated at a specific section of the propeller blade.

Assuming the flow over the propeller transitions into turbulent, we can estimate the boundary layer thickness at the trailing edge using flat plate approximation. Equation (26) is used to estimate the boundary layer thickness using flat pate approximation.

$$\delta = \frac{0.37c}{Re^{1/5}} \tag{26}$$

The foundational mathematics for serrated edges was developed by M.S. Howe (1991). His acoustic analogy proves how serrations work they cause the turbulent eddies to scatter sound at different times (decorrelation) and destructively interfere with each other.

Howe defined a Convection Velocity (U_c), which is the speed at which the turbulent eddies travel over the trailing edge. Empirically, this is roughly 60% to 70% of the freestream velocity. 65% of freestream velocity V_r is taken for convection velocity which is given by Equation (27)

$$U_c \approx 0.65V_r \tag{27}$$

Howe's theory dictates that serrations only reduce noise above a specific Crossover Frequency (f_c). Below this frequency, serrations can increase noise (a phenomenon called low-frequency penalty). The crossover frequency can be calculated using Equation (28)

$$f_c \approx \frac{U_c}{h} \tag{28}$$

In our case, for the section 75% of the radius the boundary layer thickness was calculated to 0.2 mm. Height of the serration should be greater than or at least equal to the boundary layer thickness ($h \geq \delta$). For small drones' height (h) can be taken 10% to 15% of chord length which resulted in the height of around 1.6 mm. The wavelength (λ) should also be greater than the boundry layer thickness. The calculations focus on the 50% to 90% radial stations, where serrations are most effective for noise reduction due to the higher local velocities and turbulent energy. The serration angle ($\emptyset_s$) can be calculated using Equation (29).

$$\emptyset_s = 2arctan\left(\frac{\lambda}{2h}\right) \tag{29}$$

Generally, wavelength is taken as twice of boundary layer thickness. Using these values the sharpness ratio (h/λ) was calculated which was above the constraint value of 1. Subtractive geometry design was done for the serrated edge propeller which can be seen in Figure 3.4. The final model for the serrated edged propeller can be seen in Figure 3.5. The calculated values for different sections are available in the annex section.

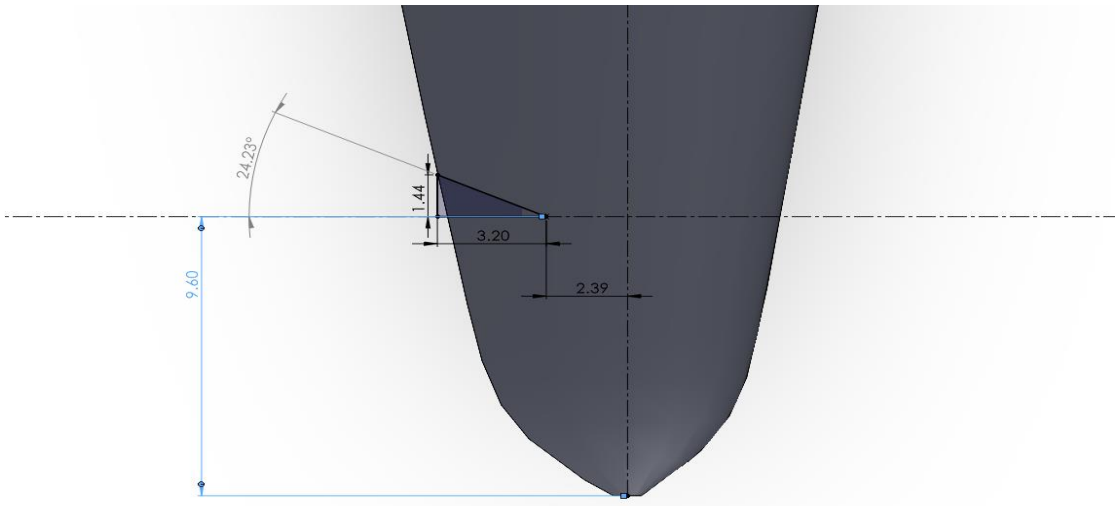

Figure 3.4: Serrated edge geometry

Figure 3.5: Serrated edged propeller

3.5.3 Dimpled Propeller Geometry

Modeling dimpled surfaces requires defining the topographical variation relative to the smooth airfoil coordinates. Geometry is typically defined by three primary parameters: Diameter (d), Depth (k), and Surface Coverage Ratio (S_c). Depth-to-Diameter ratio (γ) is the most critical non-dimensional parameter for dimple effectiveness is the ratio of depth to diameter. Experimental studies suggest that for optimal drag reduction, this ratio should fall within a specific range $\gamma \approx 0.01 \text{ to } 0.05$. If γ is too high, the dimple generates excessive recirculation, leading to parasitic drag. If it is too low, it fails to generate the necessary vertical vortices to re-energize the boundary layer.

Surface parameterization in a 3D coordinate system, a spherical dimple located at (x_0, y_0) on the airfoil surface can be modeled using the Equation (30) for a spherical cap:

$$z(x,y) = \sqrt{{R_s}^2 - (x-x_0)^2 - (y-y_0)^2} - (R_s - k) \tag{30}$$

Where R_s is the radius of the sphere from which the dimple is cut, calculated using Equation (31)

$$R_s = \frac{{d/_2}^2 + k^2}{2k} \tag{31}$$

The placement of dimples is mathematically determined by the local boundary layer thickness (δ). The dimples must be sized such that the depth k is on the same order of magnitude as the viscous sublayer or the inner region of the boundary layer. Boundary layer thickness can be calculated using Equation (32).

$$\delta = \frac{5.0x}{\sqrt{Re_x}} \tag{32}$$

To trigger transition without causing massive flow blockage, the height-to-boundary-layer ratio is often targeted at k/$\delta \approx$ 0.1 to 0.5.

Coverage and distribution of the dimples is modeled via the Surface Coverage Ratio (S_c). which represents the fraction of the airfoil surface area (A_{total}) occupied by dimples. Surface Coverage Ratio can be calculated using Equation (33)

$$A_{dimples} = \frac{\Sigma \pi \left(d/2\right)^2}{A_{total}} \tag{33}$$

Usually, a staggered (hexagonal) pattern is used rather than an aligned pattern to maximize the interaction between the generated streamwise vortices and the flow. Circular dimples are added on the top surface of the propeller. The diameter of the dimple was taken around 1% of the radius of the propeller. This diameter was selected because the geometry of the propeller was very thin and the highest span wise length was around 22mm. Instead, of creating a higher diameter circular dimples several smaller diameter dimples were added across the surface of the propeller. The depth of the dimples was set to 0.25mm. The geometry of the dimples can be seen in Figure 3.6. The spacing between the dimples is 3mm.

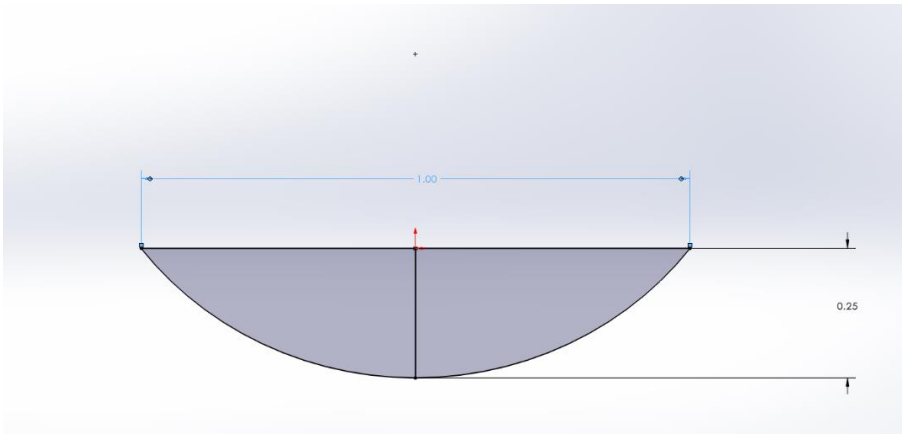

Figure 3.6: Dimple geometry

3.5.4 Serrated and Dimpled Model

The combination of both serrated and dimpled geometry is modeled and can be seen in Figure 3.7.

Figure 3.7: Serrated trailing edge and circular dimpled propeller model

3.6 Computational Analysis

Mesh will be generated for both conventional propeller and dimpled serrated propeller. Hybrid mesh with surrounding, inflation layers (y^+ = 1), and unstructured cells near the complex geometry of the propeller. For CFD analysis we will need to figure out the first layer thickness then use the inflation layer option in ANSYS fluent with expansion ration of 1.2 for the subsequent layers.

For us to calculate the first cell height we need to calculate the skin friction coefficient (C_f) which can be calculated using the following Equation (33)

$$C_f = 0.058Re^{-0.2} \tag{33}$$

After calculating the friction coefficient, we will need to calculate the wall shear stress (τ_w) which will be used to calculate the friction velocity (u_τ) using Equation (34) and (35)

$$\tau_w = \frac{1}{2}\rho {V_r}^2 C_f \tag{34}$$

$$u_\tau = \sqrt{\frac{\tau_w}{\rho}} \tag{35}$$

First cell height can be calculated using Equation (36)

$$y^+ = \frac{\rho u_\tau y}{\mu} \tag{36}$$

Where μ is the dynamic viscosity of the air.

To find the physical height for our mesh we rearrange the Equation (36) to solve it for y and take $y^+ = 1$

$$y = \frac{y^+ \mu}{\rho u_\tau} \tag{37}$$

For 75% of radius this value was found to be around $2.91e^{-6}\ m$. This value was for the initial height, and 15 layers were defined to fully capture the boundary layer.

CFD Simulations (ANSYS Fluent):

- Transient sliding mesh simulations for detailed aerodynamic performance.
- Transition SST turbulence model used for low-to-moderate Reynolds flows.

The Transition SST turbulence model was selected due to its computational efficiency and suitability for low-to-moderate Reynolds number flows where the flow isn't fully turbulent yet. However, this model has limitations in resolving highly unsteady flow features such as vortex shedding induced by sharp trailing-edge serrations. Higher-fidelity models such as LES or DES would provide improved accuracy but were beyond the computational scope of this study. The parameters used in the simulation can be found in Table 3.2. The first boundary layer was calculated to around $2.91e^{-6}\ m$, but for the computation complexity and the required cell size it was relaxed and $1e^{-5}\ m$ was taken for the first cell height.

The time step size was determined based on the frequency of propeller at 9600 RPM. Within each step the propeller was moved by 2° to keep the for the simulation to be stable. Since this was done for static test direct calculation of time step size using Courant Number using velocity wasn't possible. The time step was calculated using Equation (38)

$$TimeStep = \frac{2}{frequency \times 360°} \tag{38}$$

Table 3.2 Ansys Fluent Simulation Parameters

Parameter	Parameter Value
Propeller RPM	5000, 7500, 9600 RPM
Maximum mesh element size	50 mm
Minimum mesh element size	0.25 mm - 0.1mm
Gravity	9.81 m/s^2
Time	Transient
Time step size	0.000055
Number of time steps	1000
Number of iterations per time step	15
Viscous model	Transition SST
Near wall treatment	Correlation
Medium	Air
Specified Operating Density	1.225 kg/m^3

For ANSYS Fluent simulations the propeller must be fully enclosed in the fluid domain. The computational domain is divided into two cylindrical regions: rotational domain and stationary domain. The rotational domain was meshed using a body sizing of 4mm. Since dimples and serrations are essential features of the rotating domain and are densely distributed, a fine mesh was required in these areas. Due to the twisting nature of the propeller, structured meshing was not possible. The stationary domain has a diameter of 1.4 m, corresponding to approximately 5D (where D denotes the propeller diameter), and a height of about 13D. The rotating domain has a diameter of 1.14D and a height of 0.29D.

For the boundary condition, since this is a static test, surfaces of stationary domain are set with the boundary conditions of zero-gauge pressure outlet. The transfer of data between the static and rotational domains is exchanged via the no-slip shear boundary. The rotational speed of the propeller is set to 5000, 7500, 9600 rpm. Sliding mesh was used in cell zone and the rotational axis was set to y-axis.

3.6.1 Mesh Information

Table 3.3summarizes the mesh statistics for the base and dimpled propeller configurations. The dimpled propeller required a significantly higher cell count due to the increased surface complexity introduced by the dimples, resulting in approximately 1.5 times more elements than the base configuration. Mesh quality measures like skewness and orthogonality maintained acceptable ranges in spite of this increase, guaranteeing numerical resilience and convergence stability.

Table 3.3: Mesh Metrics for Base Propeller and Dimpled Propeller

Mesh Param	Base Propeller	Dimpled Propeller
Number of Nodes	455445	2548865
Number of Elements	682466	3803089

Dense cell clustering near blade tips, trailing edges, and surface modifications is confirmed by visual inspection of the mesh, as seen in Figure 3.8–Figure 3.12, while smooth cell transitions are maintained across the domain. These meshing qualities ensure that the primary flow phenomena, including wake formation, boundary-layer behavior, and tip vortices, are adequately resolved for comparative aerodynamic study.

Due to computational limitations, a formal grid-independence study was not carried out; however, convergence behavior, stable force histories, and constant quantitative agreement between CFD predictions and experimental trends validated the chosen mesh resolution. For the objectives of this study, the mesh method used thus offers reliable compromise between numerical precision and computing efficiency.

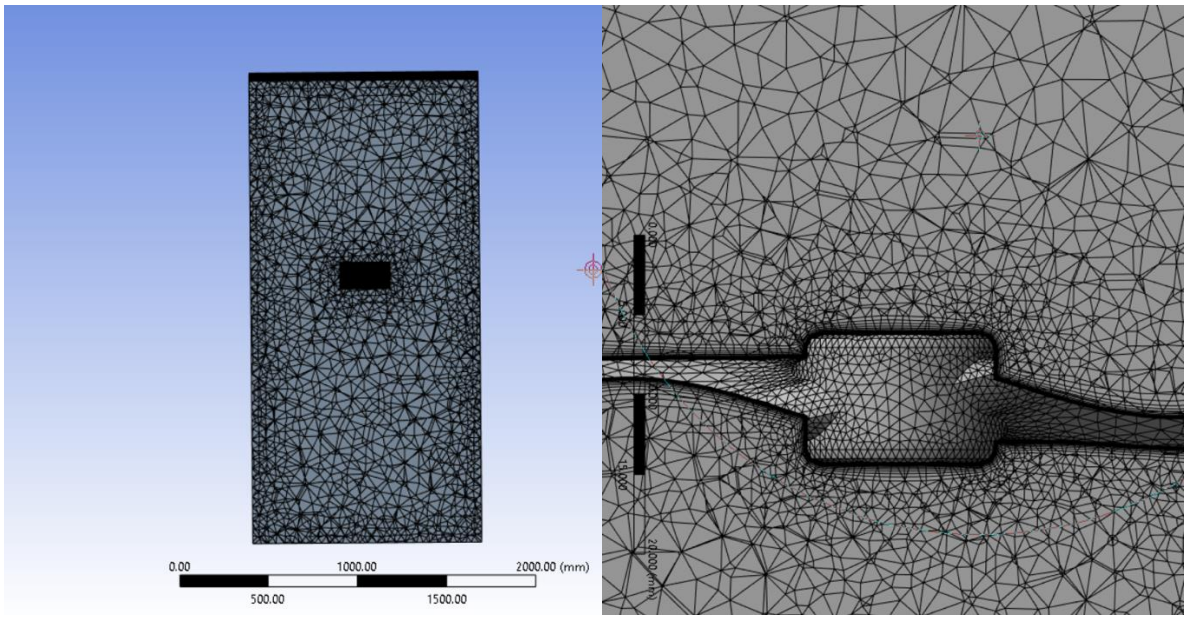

Figure 3.8: Mesh of the propeller

Figure 3.8 shows the mesh of the propeller and its stationary domain. On the left we can see the stationary domain within which the rotational domain lies. The rotational domain was given a body size of 4mm and due to which the mesh is much denser in the rotational domain. The

inflation layers on the propellers can be seen on the right and the mesh around the propeller can also be seen clearly.

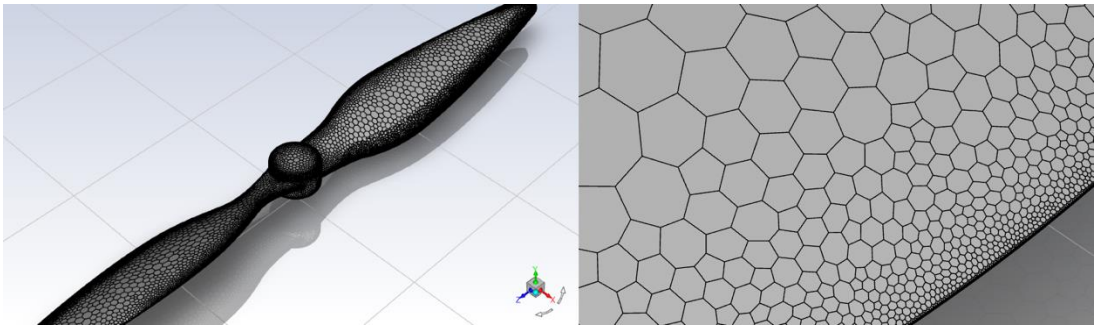

Figure 3.9: Base Propeller Polyhedral Mesh showing smaller elements at the tip

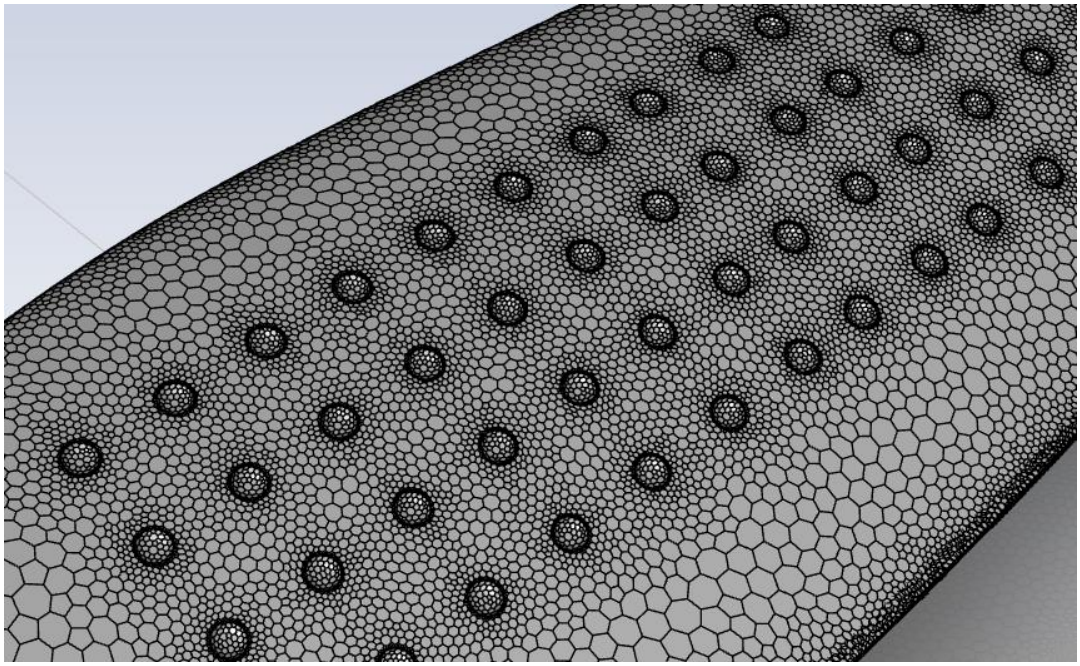

Figure 3.10: Dimpled Propeller Polyhedral Mesh showcasing tight meshing around the dimples and edges

Error Check	Quality Criterion	Warning Limit	Error (Failure) Limit	Worst
☐	Max Aspect Ratio	Default (5)	Default (1000)	10.521
☐	Min Element Quality	Default (0.05)	Default (5e-04)	0.215
☐	Min Orthogonal Quality	Default (0.05)	Default (5e-03)	0.201
☐	Max Skewness	Default (0.9)	Default (0.999)	0.799

Figure 3.11: Base Propeller Mesh Quality

Error Check	Quality Criterion	Warning Limit	Error (Failure) Limit	Worst
☐	Max Aspect Ratio	Default (5)	Default (1000)	9.422
☐	Min Element Quality	Default (0.05)	Default (5e-04)	0.225
☐	Min Orthogonal Quality	Default (0.05)	Default (5e-03)	0.152
☐	Max Skewness	Default (0.9)	Default (0.999)	0.848

Figure 3.12: Dimpled Propeller Mesh Quality

3.7 Experimental validation of the simulation results

Numerically simulated data using computational fluid dynamics (CFD) will be compared with the data gathered through experimental testing. During validation we will see if experimental testing shows comparable results with the CFD simulations we performed for both conventional and dimpled serrated propellers.

During the printing of propellers due to the minute structures as well and complex shape the conventional 3D filament printing wasn't possible. In the Figure 3.13, we can see that there are severe imperfections on the propeller and the serrated edges are not properly printed. After failure with filament, resin printing was chosen which resulted in a much better structure. In Figure 3.14, the resin printed propeller compared side by side to a commercially available 8 inch propeller. The commercially available propeller has the number 8045 and is made from composite material including nylon. We can see all the resin printed propellers with the commercial one in Figure 3.14. The mechanical properties of the resin used in propeller printing are listed in Table 3.4.

Table 3.4: Mechanical Properties of the Resin (ANYCUBIC n.d.)

Hardness	81-83 HD
Tensile Strength	35-45 MPa
Elongation at Break	23-30%
Bending Modulus	45-55 MPa
Bending Strength	2200-2500 MPa
Young's Modulus	1300-1500 MPa
Volume Shrinkage Rate	2-3%

For the experimental setup and stand was 3D modeled and manufactured. The stand was made from mild steel pipe with a dimension of 1 inch. The complete model of the stand and final manufactured stand can be seen in Figure 3.16 and Figure 3.22. The stand with all the sensors

attached to it can be seen in Figure 3.22. The sensors are powered by a 5V 1A DC power adapter.

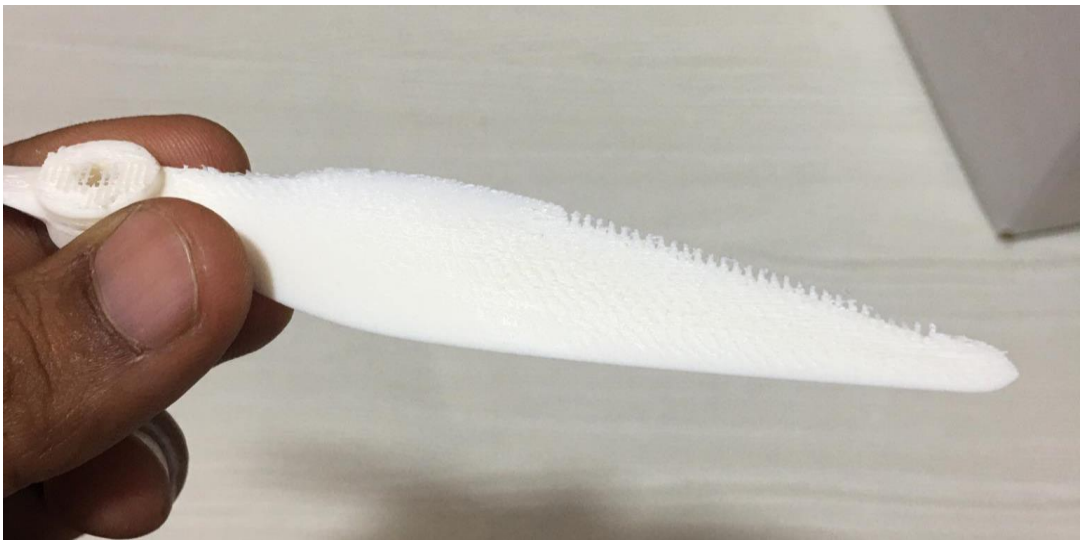

Figure 3.13: PLA prop with severe imperfections

Figure 3.14: Commercially available propeller on the left and resin printed one on the right

Figure 3.15: Resin Printed Propellers and commercial propeller

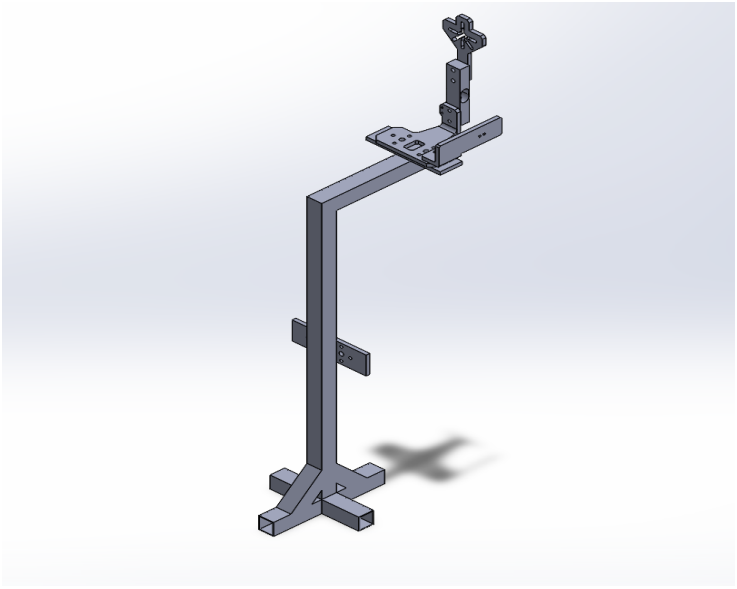

Figure 3.16: Stand assembly

3.7.1 Sensors and Microcontrollers

3.7.1.1 Load Cell

For the measurement of thrust generated by the propellers load cell is used. Load cell is a mechanical transducer that converts mechanical force such as (tension, compression, or torque) into a measurable, standardized electrical signal. Figure 3.17 shows the load cell with deformation and the change in resistance due to deformation is what load cell measures.

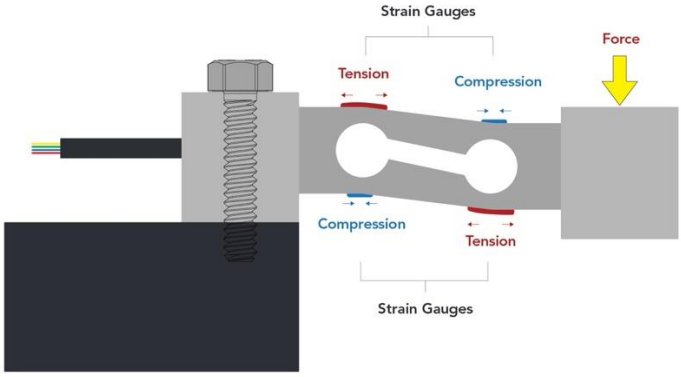

Figure 3.17: Load cell with deformation (Anyload 2024)

Primarily used for precise weighing in industrial, commercial, and laboratory applications, they typically utilize strain gauges, hydraulic, or pneumatic mechanisms to measure loads, providing high accuracy, often between 0.01% and 0.05%.

A strain gauge load cell converts force into an electrical signal by means of precision strain gauges, which alter their resistance in response to applied pressure or load. The strain gauge and the sensing element are the two main parts of a strain gauge load cell which allow this conversion.

- Strain gauges: A type of variable resistor that changes in resistance output in proportion to the deformation of the metal.
- Element: A machined piece of metal that responds predictably in proportion to an applied force.

The strain gauge load cell's core is formed by the strain gauges, which are precisely adhered to the sensing element.

To amplify their sensitivity and accuracy, strain gauges are integrated into a Wheatstone Bridge circuit. This circuit enhances the load cell’s ability to detect minute changes in resistance, thereby allowing for exceptionally precise measurements (Anyload 2024). To measure the thrust generated by the propellers a 5kg load cell was used.

3.7.1.2 IR Sensor

An Infrared light-emitting diode (IR LED) is a special-purpose LED that emits infrared rays ranging from 700 nm to 1 mm wavelength. Different IR LEDs may produce infrared light of

differing wavelengths, just like other LEDs produce light of different colors. IR sensor is a device that uses infrared technology to detect objects or changes in the environment. IR sensors can detect a wide range of physical properties such as temperature, motion, and proximity (Efyian 2024).

The appearance of an IR LED is the same as a common LED. Since the human eye cannot see infrared radiation, it is not possible for a person to identify if an IR LED is working. To measure the RPM of the propellers active type of IR sensor is used, which means the senor will emit and receive the reflected infrared light to check if the propeller blades are in front of the sensor or not.

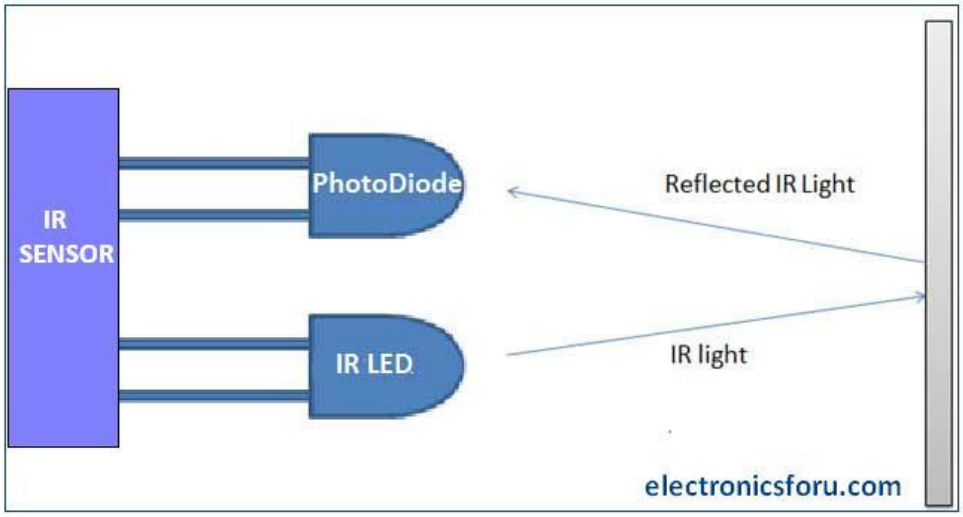

Figure 3.18: IR sensor working principle (Efyian 2024)

To calculate the RPM digital signals created over a time interval e.g., 1 second or 1000ms) are counted and RPM is calculated by using the formula

$$RPM = (pulse\ count/num\ of\ blades) * 60 \quad (38)$$

Counting the pulses in a second and multiplying it by 60 works for slow RPM's but for higher RPM's this will not work and give inaccurate values. To counteract that, the pulses are counted for specific sampling rate time, which in our case of 20Hz is around 50 milliseconds. The pulses are counted and the value is copied then reset and count over a second. After this the values are extrapolated based on that.

3.7.1.3 Microcontroller

For the control of sensors and reading of data from the sensors a microcontroller is required. Arduino UNO was selected as the microcontroller for this purpose. Arduino Uno is a microcontroller board based on the ATmega328P. It has 14 digital input/output pins (of which 6 can be used as PWM outputs), 6 analog inputs, a 16 MHz ceramic resonator (CSTCE16M0V53-R0), a USB connection, a power jack, an ICSP header and a reset button. It contains everything needed to support the sensors, and display output for our case.

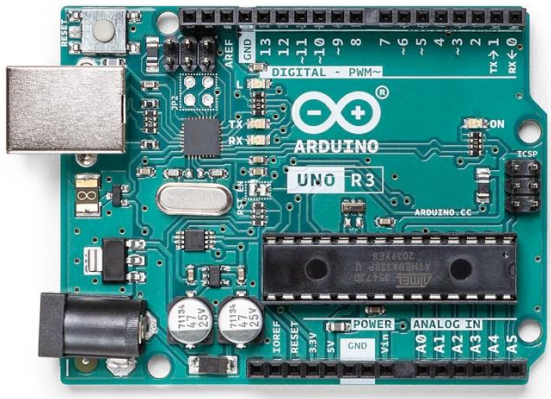

Figure 3.19: Arduino UNO Microcontroller (Arduino n.d.)

3.7.1.4 LCD Display

For the reading of sensor data liquid crystal display is used. The LCDs have a parallel interface, meaning that the microcontroller must manipulate several interface pins at once to control the display. The interface consists of the following pins:

- Register select (RS): This pin controls where in the LCD's memory, you're writing data to. You can select either the data register, which holds what goes on the screen, or an instruction register, which is where the LCD's controller looks for instructions on what to do next.
- Read/Write (R/W): This pin selects reading mode or writing mode
- Enable: This pin that enables writing to the registers
- 8 data pins (D0 -D7): The states of these pins (high or low) are the bits that you're writing to a register when you write, or the values you're reading when you read.

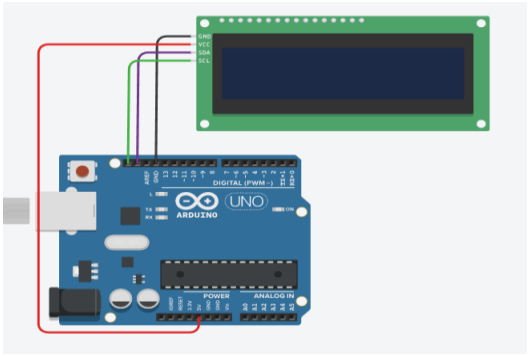

Figure 3.20: LCD display interfacing with Arduino UNO microcontroller (GeeksforGeeks 2023)

The display will be used to show the thrust values generated by the load cell and the RPM values generated by the IR sensor. RPM and Thrust will get displayed in separate rows of the display.

3.7.1.5 Hall effect Sensor

Hall effect sensor (also known as Hall Sensor) has also been used to measure the RPM of the propeller. It works on the Hall effect principle, in which a voltage is produced proportional to the axial component of the magnetic field. Hall effect sensors are primarily used for positioning, proximity sensing, speed detection and current sensing applications. In this study a magnet is attached to the body of the rotor and hall effect sensor is placed near it. The moment magnet passes over it a signal is generated which is read out by the microcontroller.

3.7.1.6 Current and Voltage Sensing modules

For the measurement of current and voltage, ACS712 module and generic voltage sensing module were utilized respectively. The ACS712 module came with a rating of 20A, and the voltage sensing module came with a rating up to 25V. These modules were connected to the power line coming from a Li-Po battery and their signal wires were connected to the microcontroller for the readout. All the sensors used in the experimental setup are listed in Table 3.5. The sampling rate for used for the study was 20Hz. This sampling rate was choosen based on the sensors data gathering frequency.

Table 3.5: Sensor Details

Sensor	Rating
Load Cell with HX711 module	5kg
IR Sensor	-
Hall Effect Sensor	-
Voltage Sensing Module	5-25V
Current Sensing module (ACS712)	20A

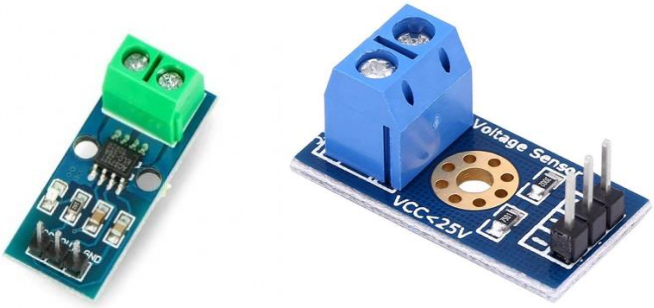

Figure 3.21: ACS712 module on the left and Voltage sensing module on the right

The complete experimental stand with all the sensors attached to it can be seen in Figure 3.22. The sensors are powered by 5V 1A DC power adapter and the motor is powered by a Li-Po battery.

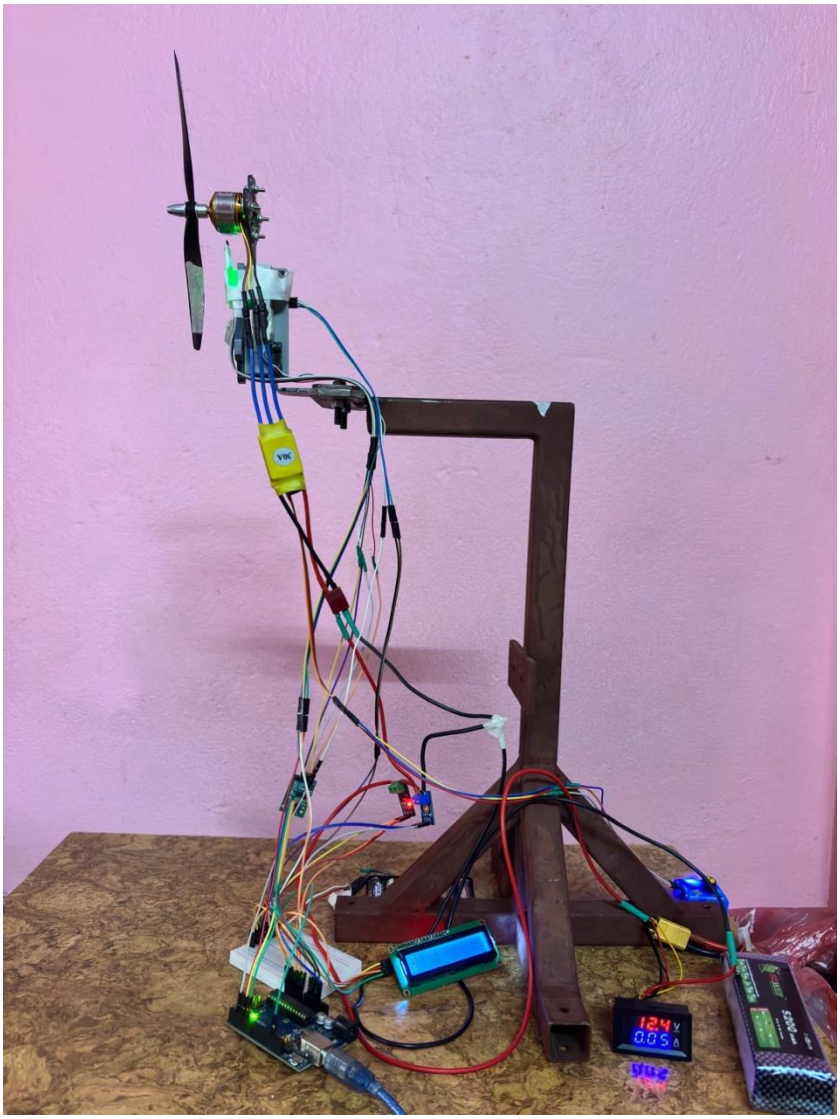

Figure 3.22: Stand with motor and load cell and all sensors mounted

CHAPTER FOUR:
RESULT AND DISCUSSION

4.1 Thrust comparison among propellers

While non-dimensional performance coefficients such as thrust coefficient and power coefficient were not explicitly calculated, all propellers were tested under identical geometric dimensions and operating conditions. Therefore, direct comparison of thrust and power trends remains valid for relative performance evaluation. Since this was a static test the efficiency of the propeller was considered using the power consumption of motor is valid.

Thrust generated by propellers at different RPM are shown in Figure 4.1. The commercially available composite propeller generated the highest amount of thrust. This seems to be due to thinner airfoil shape, smoother surface and tip geometry. Figure 4.1 compares the thrust and efficiency characteristics of different propeller configurations across a range of rotational speeds. Figure 4.1(a) demonstrates that thrust increases non-linearly with RPM for all propellers, consistent with propeller momentum theory.

(a) (b)

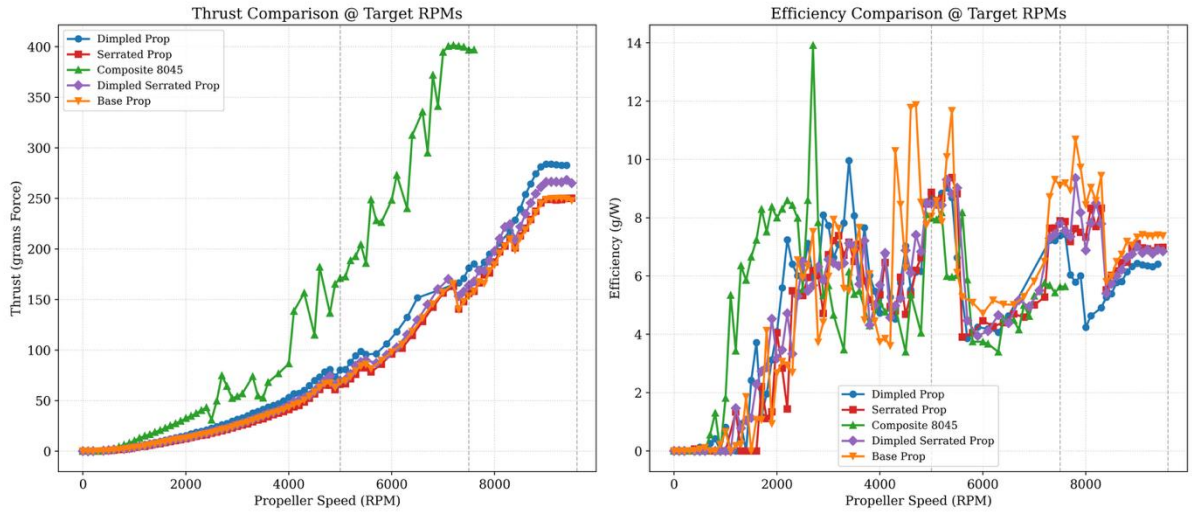

Figure 4.1: Thrust and Efficiency Comparison of all the propellers

Because of its refined blade tip geometry, improved surface smoothness, and optimized airfoil profile, the commercially available composite propeller generates the highest thrust. The dimpled propeller consistently produces more thrust compared to the baseline and serrated

configurations among the 3D-printed test models, suggesting increased aerodynamic performance because of delayed boundary-layer separation.

The efficiency trends are illustrated in Figure 4.1(b), which shows that efficiency rises with RPM up to an ideal range before stabilizing or slightly falling at higher speeds. The efficiency of the dimpled propeller is higher than that of the base propeller, indicating that the increased skin-friction losses resulting from surface dimples are outweighed by the decrease in pressure drag.

The maximum thrust produced by each propeller arrangement is listed in Table 4.1, along with the associated RPM and power consumption. The highest thrust output is achieved by the composite 8045 propeller, demonstrating the impact of advanced manufacturing techniques and improved material characteristics. The lowest thrust is generated by the base resin-printed propeller, highlighting the constraints imposed by simpler shape and surface roughness.

Table 4.1: Maximum Thrust generated by Propellers

Propeller	Max Thrust (g)	RPM at Max Thrust	Power at Max (W)
Composite Propeller (8045)	401.4	7600	74.9
Base Propeller	250.2	9300	35.4
Dimpled Propeller	283.9	9000	46.6
Serrated Propeller	250.1	9500	36.7
Serrated and Dimpled Propeller	272.7	9500	40.6

The effectiveness of surface dimples in delaying boundary-layer separation is supported by the dimpled propeller's 13–15% higher maximum thrust when compared directly to the base propeller at similar RPM levels. While the combination dimpled-serrated propeller exhibits intermediate performance, generating marginally less thrust than the simply dimpled design but greatly outperforming the baseline propeller, the serrated propeller only slightly surpasses the base version.

Thrust values from ANSYS Fluent simulations and thrust measured empirically at specific RPMs are compared in Table 4.2. Because of idealized boundary conditions, a lack of surface roughness modeling, and the CFD model's disregard for structural deformation, the calculated thrust values for propellers are consistently greater than experimental data.

Improved agreement at greater rotational speeds is indicated by the percentage error decreasing as RPM increases. Because of numerical instability, especially for serrated configurations, simulated results are not entirely available for dimpled-serrated propellers. This demonstrates the challenge in resolving intricate unsteady flow structures caused by acute serrations using the Transition SST model. The percentage inaccuracy remains between 4 and 7%, suggesting better agreement across different rotational speeds.

Table 4.2: Experimental and Simulated Data at 5000, 7500, 9600 RPM

	RPM								
	5000			7500			9600		
Propeller Name	ANSYS Fluent	Experimental	Error %	ANSYS Fluent	Experimental	Error %	ANSYS Fluent	Experimental	Error %
Base Propeller	72.59	69.03	4.9	161.67	153.34	5.15	265.15	247.85	6.5
Dimpled Propeller	86.25	80.31	6.8	189.42	181.15	4.36	295.30	282.72	4.26
Serrated Propeller	70.51	66.04	6.33	164.57	156.066	5.16	269.45	250.12	7.17
Serrated and Dimpled Propeller	NA	71.20		NA	169.12		NA	272.40	

Table 4.2 does not contain the CFD data for the serrated-dimpled propellers. When applied to sharp trailing-edge serrations, the selected turbulence modeling approach has limitations, which are shown in the lack of numerical data. Higher-fidelity turbulence models, like Large Eddy Simulation (LES) or Detached Eddy Simulation (DES), and much finer mesh resolution are necessary for the extremely unstable wake and flow separation caused by serrated edges, however these were outside the computing capabilities of this work.

Additionally, in inertia-dominated flow regimes, the percentage error systematically drops with increasing RPM, indicating better agreement between CFD and experimental results. This pattern implies that at lower rotational speeds, viscosity and surface-related effects which are not fully captured numerically play a more crucial role.

Furthermore, the resin-printed propellers may undergo slight aeroelastic deformation at higher RPMs, while the CFD calculations assume rigid blades. In experimental conditions, this deformation reduces thrust by changing the effective pitch angle and local angle of attack. The numerical models do not specifically model these effects, hub-blade junction losses, or motor-induced inflow disruptions.

Overall, Table 4.2 shows that although CFD offers useful quantitative insight into propeller performance trends, utilizing idealized geometry and simplified turbulence models is predicted to result in quantitative differences with actual results. The comparison highlights the significance of experimental validation and shows that, despite absolute variances in thrust magnitude, the numerical forecasts accurately reflect performance trends, especially at higher RPMs.

4.2 Base Propeller

Resin printing was utilized to fabricate the base propeller, which served as the baseline prop for passive surface alterations. When compared to other propellers, the base propeller produced the least amount of thrust, which was approximately 250.2g. Figure 4.2 shows the basic propeller's performance analysis. The thrust produced is essentially insignificant at lower RPM.

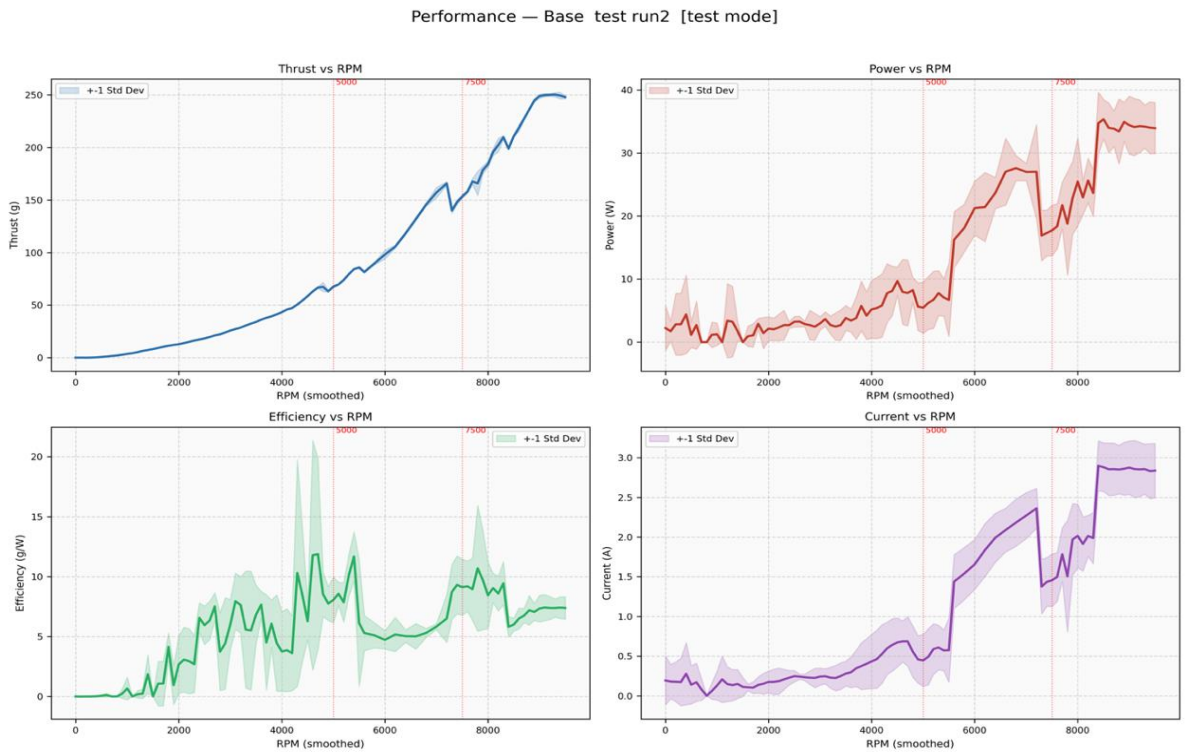

Figure 4.2: Thrust and Power comparison with RPM of Base Propeller

An infrared sensor and a hall effect sensor were employed to measure the RPM. To trigger the hall effect sensor each time the rotor completes a rotation, a magnet was secured to the rotor's shaft. The deviation values are shown by the banded region surrounding the curve.

At higher speeds, the power curve rises more sharply than the thrust curve, indicating an increase in mechanical and aerodynamic losses. The deviation band's spread represents

measurement uncertainty, which is mostly caused by variations in motor performance under load and current sensors sensitivity.

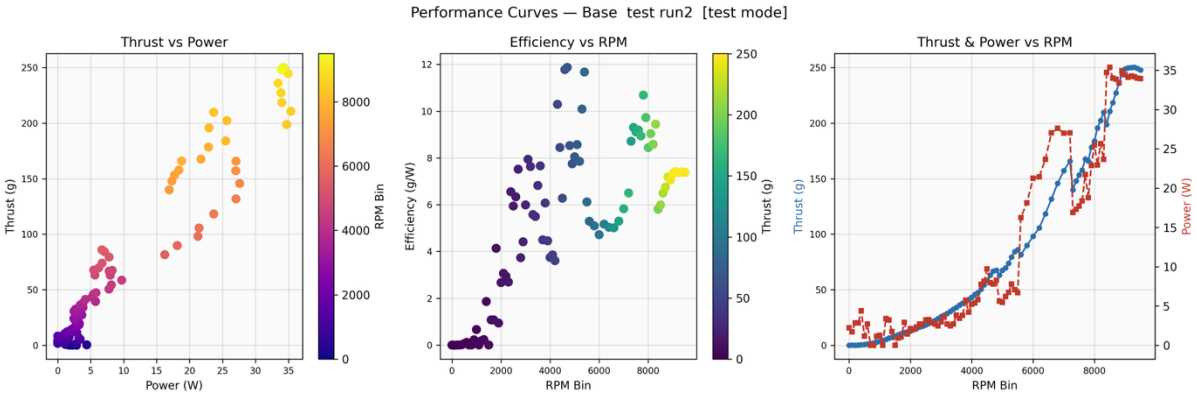

Figure 4.3: Performance Curves for Base Propeller

The usual base propeller performance curves are shown in this diagram, which also illustrates how thrust, power, and efficiency change with RPM. The efficiency curve increased steadily with RPM until it reached a moderate operating range, at which point it plateaued. The base propeller's overall aerodynamic efficiency is limited due to early boundary layer separation and greater pressure losses caused by the absence of passive flow control elements.

The basic propeller continuously generated the least thrust and efficiency when compared to the modified configurations, highlighting the disadvantages of smooth, unaltered blade surfaces under low Reynolds-number working circumstances.

4.2.1 Base Propeller ANSYS FLUENT Simulation

Figure 4.4 illustrates the flow generated by the propeller, with the peak velocity reaching approximately 69.58 m/s at 5000 RPM. This maximum speed is observed at the propeller's tip. A plane positioned 15mm beneath the propeller is established, from which streamlines are drawn. The helical trajectory of these streamlines is depicted in Figure 4.4.

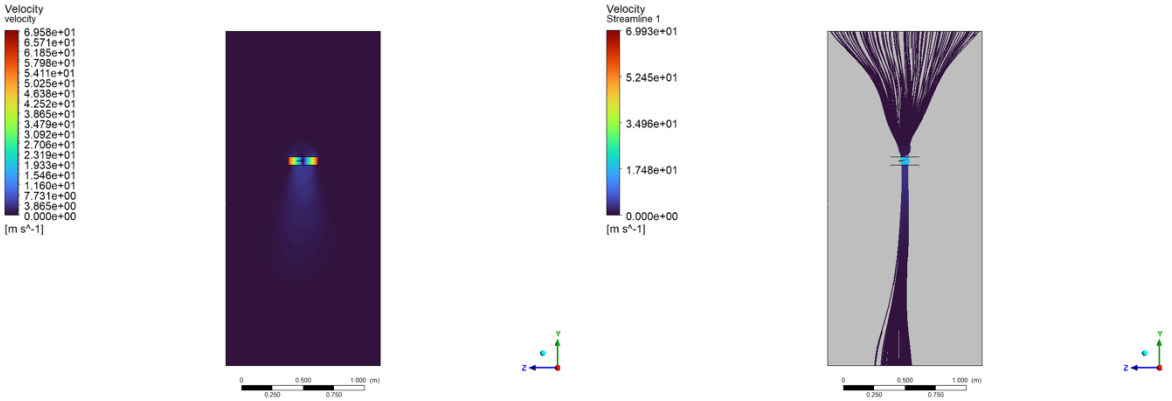

Figure 4.4: Base Propeller velocity contour and streamline at 5000RPM

Aerodynamic losses and noise are generated by rotational wake formation, which is shown by the helical streamlines downstream of the propeller. The significantly decreased thrust generation can be explained by the presence of flow separation areas close to the blade trailing edge. A comparatively moderate flow intensity across the computational domain is shown in Figure 4.5.

High-velocity areas are mostly limited to the blade passages and near the close vicinity of the trailing edges, where rotational motion causes fluid acceleration. A smooth velocity gradient is indicated by the contour plot's gradual color shift, which suggests steady flow development with few sudden changes in momentum. The velocity curve for 7500 RPM displays a maximum velocity of 110.9 m/s. The velocity increased by about 59.3% as compared to 5000 RPM.

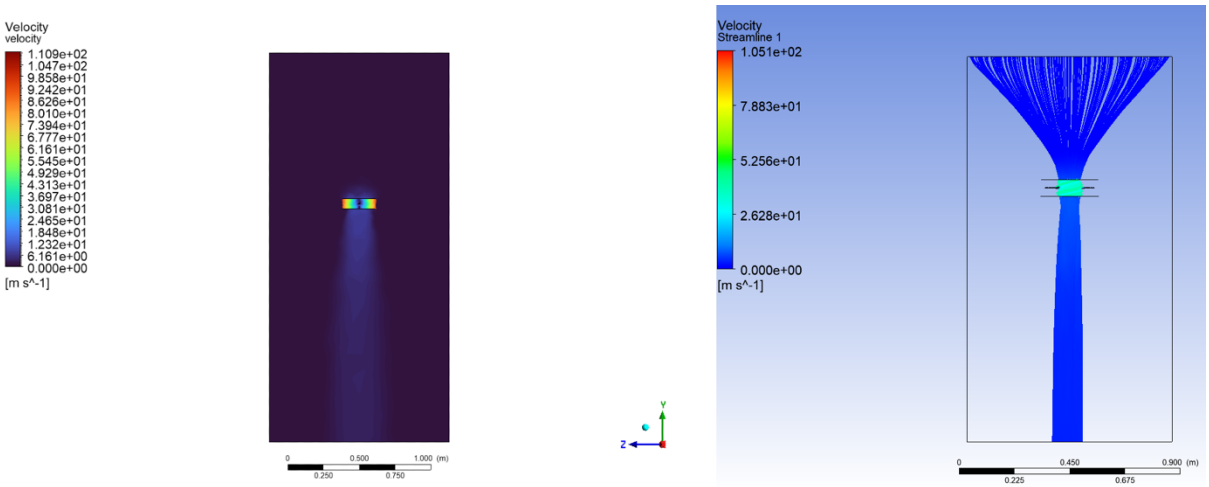

Figure 4.5: Base Propeller Velocity Contour and Streamline at 7500 RPM

Figure 4.6 shows the velocity contour of base propeller at 9600 RPM. The peak velocities are always intensified near the tips along the primary flow channel, reflecting the increased

centrifugal and inertial forces. At 9600 RPM the maximum velocity jumps to 139.2 m/s, which approximately 25.5% increase over 7500 RPM.

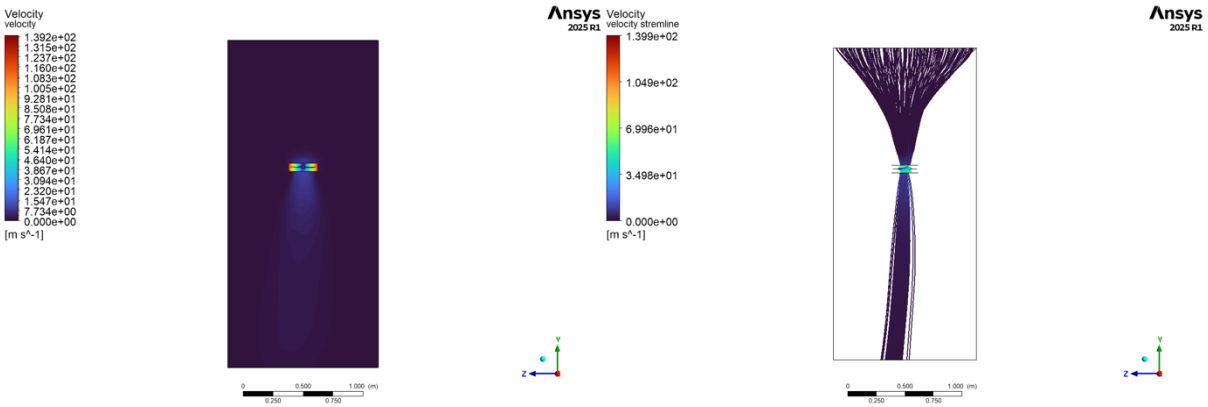

Figure 4.6: Base Propeller Velocity Contour and Streamline at 9600 RPM

4.3 Serrated Propeller

Propeller with serrations added to the trailing edge performed slightly worse than the base propeller. In our case, if we compare the serrated propeller and base propeller thrust values at 5000 RPM, we get a difference of around 4.33%. This comes close to what was seen in the study conducted by (Gu, et al. 2024), where the serrated propeller generated slightly lower thrust around 4 - 6% than the one with no serrations added to them. The performance analysis of serrated propeller can be seen in Figure 4.7.

This phenomenon can be explained by better wake mixing and delayed vortex shedding brought on by serration geometry, which deviates from trends in some literature. The serrated propeller, however, exhibits greater power efficiency variation, indicating that serrations modify both wake structure and aerodynamic loads.

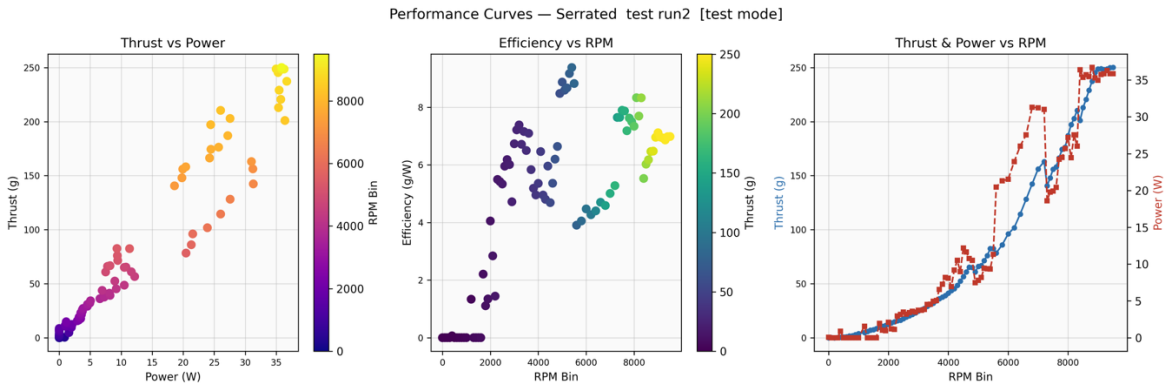

Figure 4.7: Performance Curves for Serrated Propeller

The serrated propeller's thrust and power curves are compared across RPM in Figure 4.8. Although thrust somewhat increases in comparison to the base propeller, power consumption is still relatively low. The lower power required suggests that aerodynamic stresses may be redistributed along the blade span to reduce induced losses.

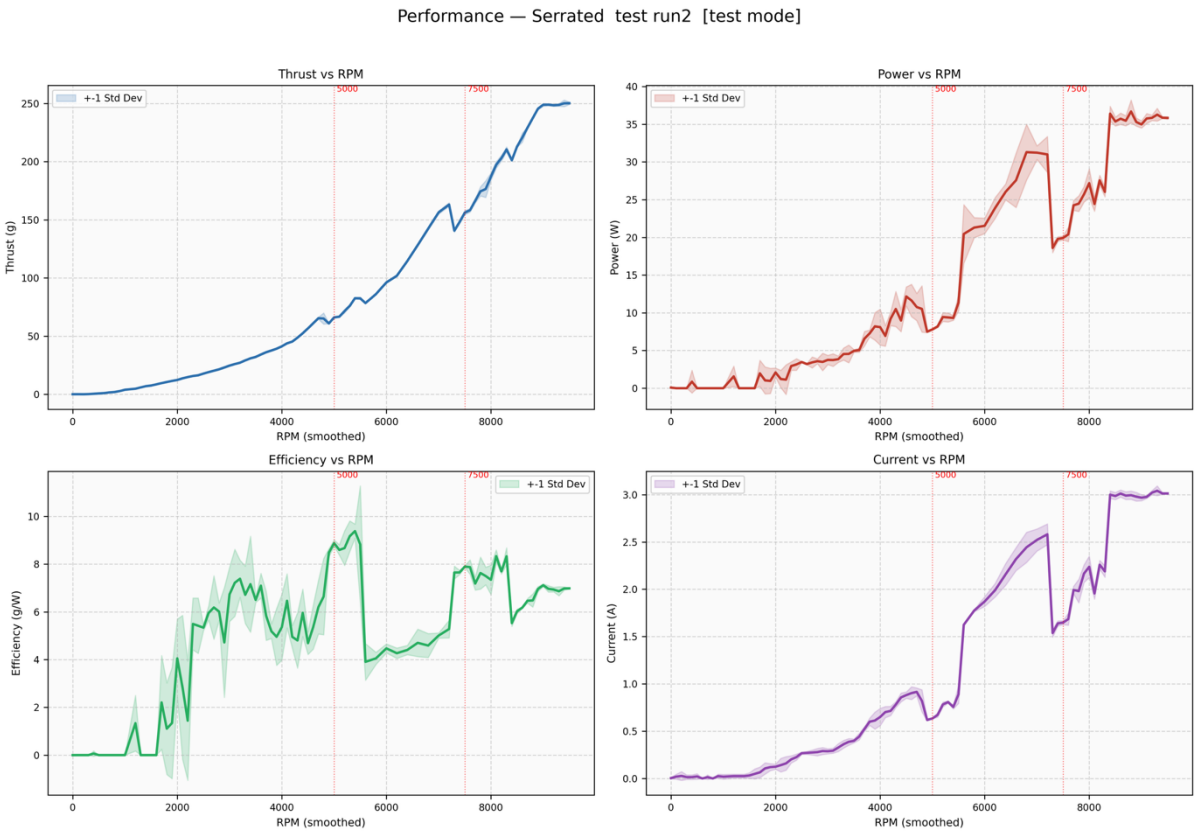

Figure 4.8: Thrust and Power comparison with RPM of Serrated Propeller

4.3.1 Serrated Propeller ANSYS FLUENT Simulation

The flow from the propeller can be seen in Figure 4.9 and the maximum velocity at 5000 RPM is around 86.32 m/s. The highest velocity occurs at the tip of the propeller. A plane 15mm below the propeller is created and the streamlines are drawn from it. We can see the helical path of the streamlines in Figure 4.9.

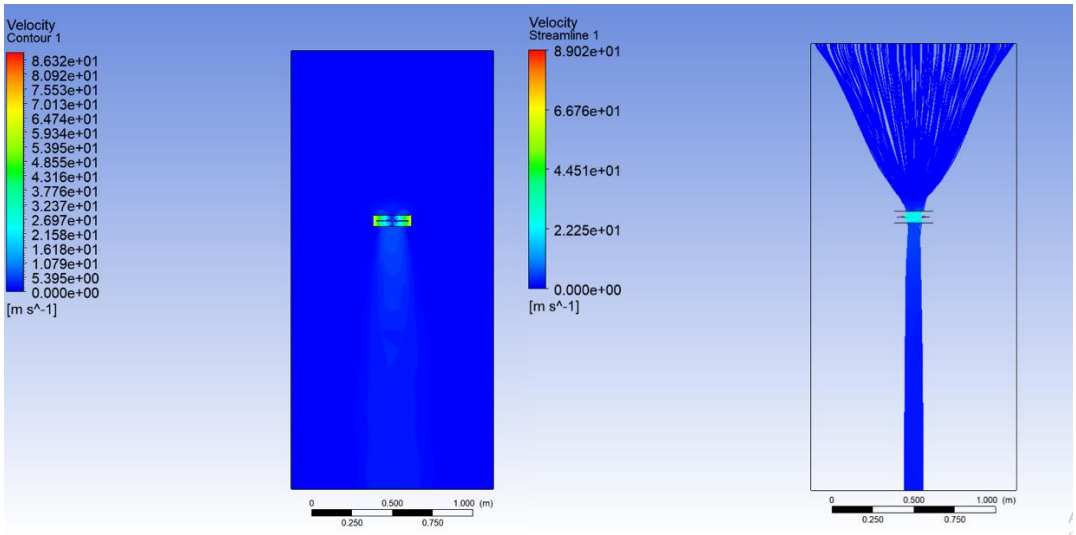

Figure 4.9: Serrated Propeller velocity contour and streamline at 5000RPM

The helical streamlines downstream of the propeller indicate rotational wake development, which contributes to aerodynamic losses and noise generation. Flow separation regions near the blade trailing edge are visible, explaining the comparatively lower thrust production.

Figure 4.10 illustrates a relatively moderate flow intensity throughout the computational domain. High-velocity regions are primarily confined to the blade passages and near the trailing edges, where fluid acceleration occurs due to rotational motion. The gradual color transition in the contour plot indicates a smooth velocity gradient, suggesting stable flow development with limited abrupt changes in momentum. The maximum velocity shown in velocity contour for 7500 RPM is around 136 m/s. Compared to 5000 RPM the velocity increased by approximately 57.55%.

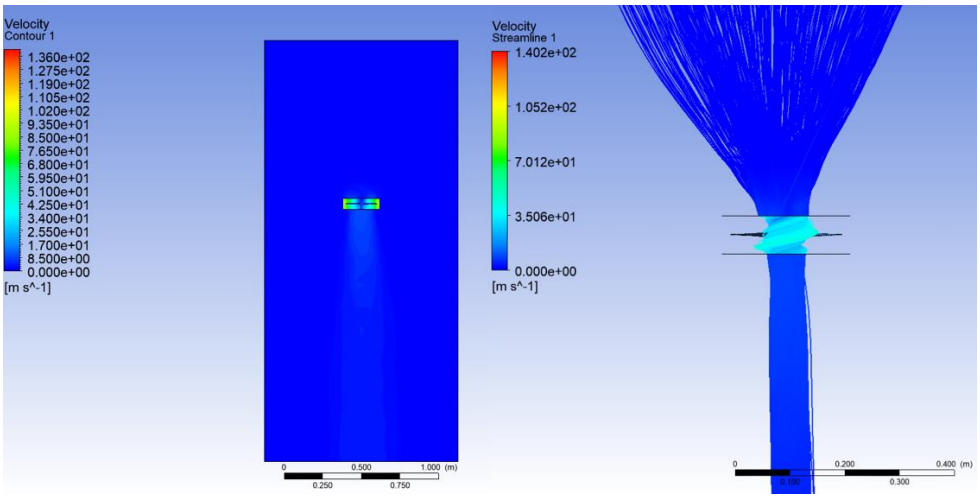

Figure 4.10: Serrated Propeller Velocity Contour and Streamline at 7500 RPM

Figure 4.11 shows the velocity contour of base propeller at 9600 RPM. The peak velocities are always intensified near the tips along the primary flow channel, reflecting the increased centrifugal and inertial forces. At 9600 RPM the maximum velocity jumps to 181.3 m/s which is approximately 33.33% increase over 7500 RPM.

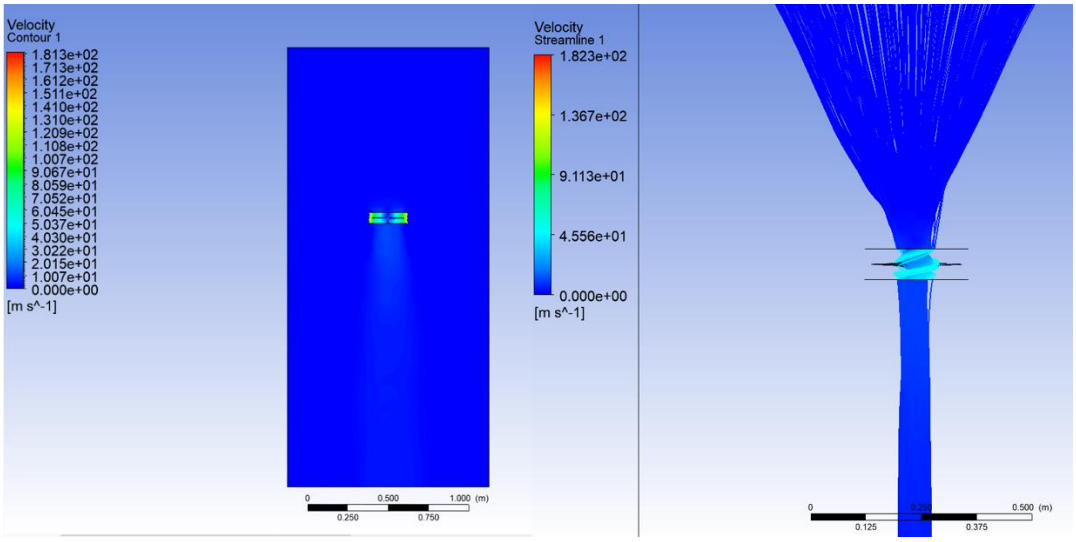

Figure 4.11: Serrated Propeller Velocity Contour and Streamline at 9600 RPM

4.4 Dimpled Propeller

Circular dimples were added to the upper surface of the propeller, covering around 50 - 60% of the surface with a cut of 0.25mm. These dimples were added to the propeller to help in recirculation of air when it passed through them causing the boundary layer to stay attached and reduced premature boundary layer separation. Dimples on the surface can reduce the drag coefficient by significant amount, around 6.6% in the best-case scenario (Ali, et al. n.d.).

In our study we found that dimpled propeller performed well compared to the base, serrated, and serrated and dimpled propeller. The maximum amount of thrust generated by the dimpled propeller was 283.9g at 9000 RPM, which is the average value across 3 sample readings. This constitutes an approximately 13.4% increase in thrust generation over the base propeller. The performance of dimpled propeller can be seen in Figure 4.12.

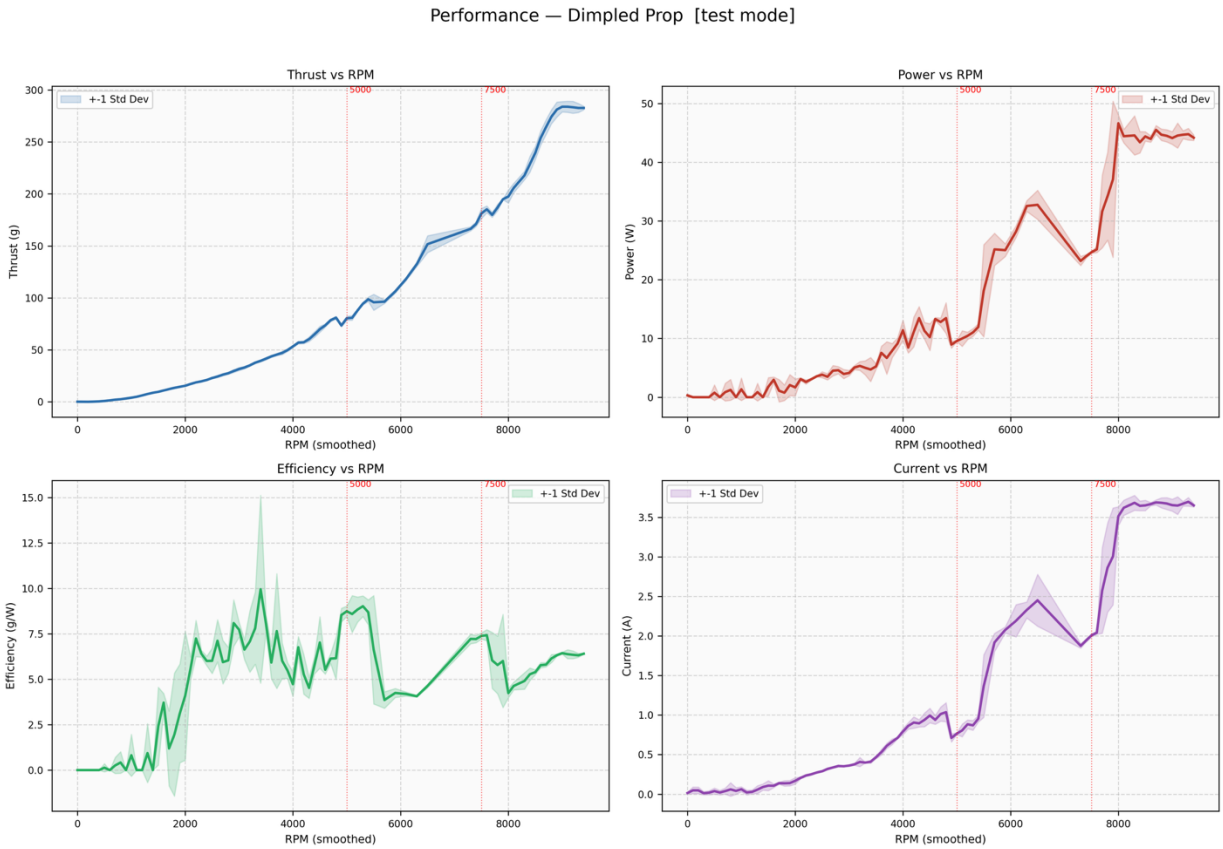

Figure 4.12: Thrust and Power comparison with RPM of Dimpled Propeller

Figure 4.13 demonstrates that the dimpled propeller produces a consistently higher thrust across the tested RPM range compared to all other resin-printed propellers. The increase in thrust becomes more pronounced at higher RPM values, indicating that dimples are particularly effective in high-speed operating regimes. The power curve shows a moderate increase relative to the base propeller, confirming that the thrust gains are achieved primarily through pressure drag reduction rather than increased energy input.

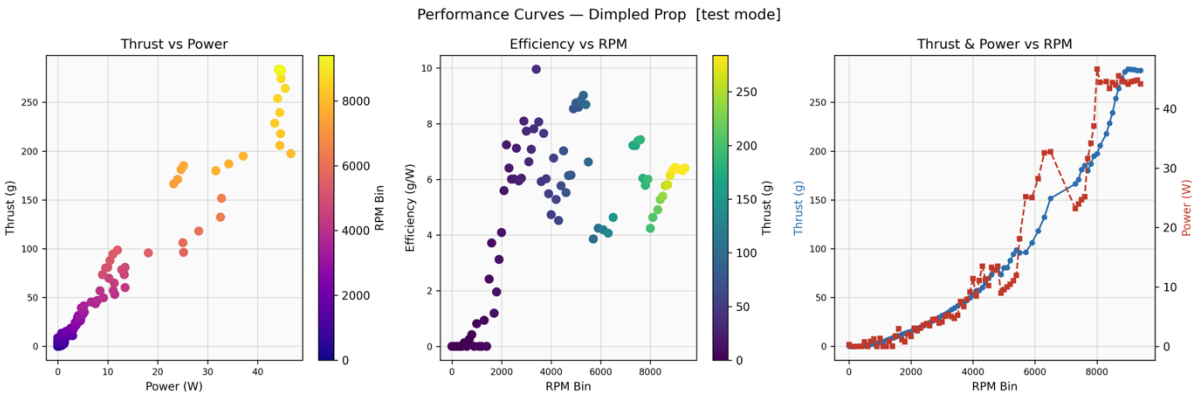

Figure 4.13: Dimpled Propeller Performance Curves

The enhanced aerodynamic efficiency of the dimpled propeller is demonstrated by the performance curves in Figure 4.13. A more advantageous thrust-to-power ratio is shown by the efficiency trend, particularly at mid-to-high RPM levels. This enhancement supports the theory that laminar separation bubbles are suppressed, and the boundary layer is energized by surface dimples.

4.4.1 Dimpled Propeller ANSYS FLUENT Simulation

The flow field surrounding the dimpled propeller at 5000 RPM is shown in Figure 4.14. The wake shows less separation intensity, and the velocity distribution is more consistent along the blade surface than with the base propeller.

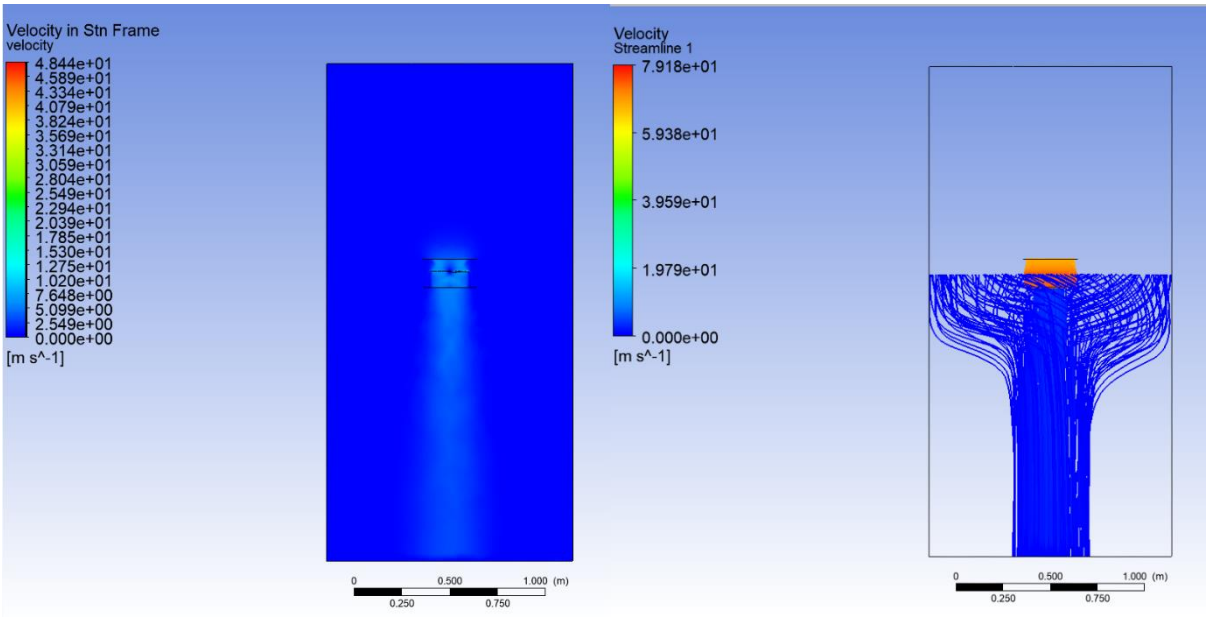

Figure 4.14: Dimpled Propeller Velocity Contour and Streamline at 5000 RPM

Improved momentum transfer to the airflow is indicated by the maximum velocity (≈79.18 m/s), which is higher than that of the base propeller. The observed increase in thrust is supported by the streamlines' enhanced flow attachment. Because of better boundary-layer control and less flow separation, the dimpled arrangement outperforms both the base and serrated propellers in terms of thrust generation and efficiency, especially at higher RPMs.

The dimpled propeller's streamline and velocity profile at 7500 RPM are displayed in Figure 4.15. The maximum speed is roughly 111.8 m/s, which is greater than the basic propeller's velocity at 7500 RPM. The streamline portion of Figure 4.15 shows the helical path and air stream leading to the output.

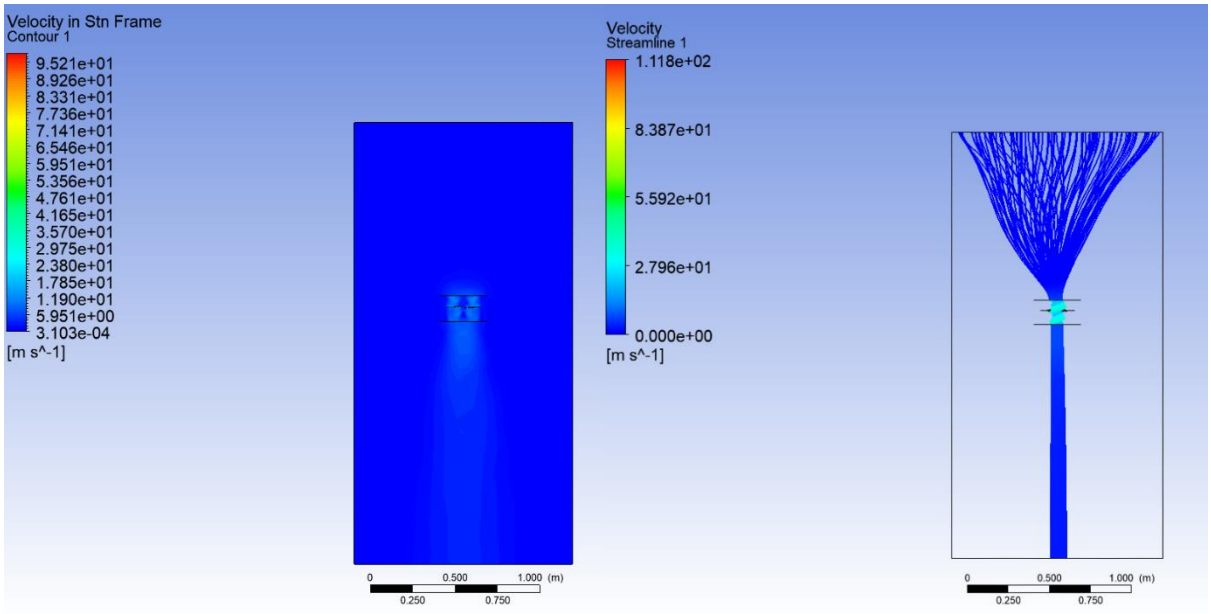

Figure 4.15: Dimpled Propeller Velocity Contour and Streamline at 7500 RPM

The dimpled propeller's velocity profile and streamline at 9600 RPM are displayed in Figure 4.16. The highest velocity is roughly 141.8 m/s, which is greater than the base propeller's velocity at 9600 RPM. The streamline portion of Figure 4.16 shows the helical path and air stream leading to the output.

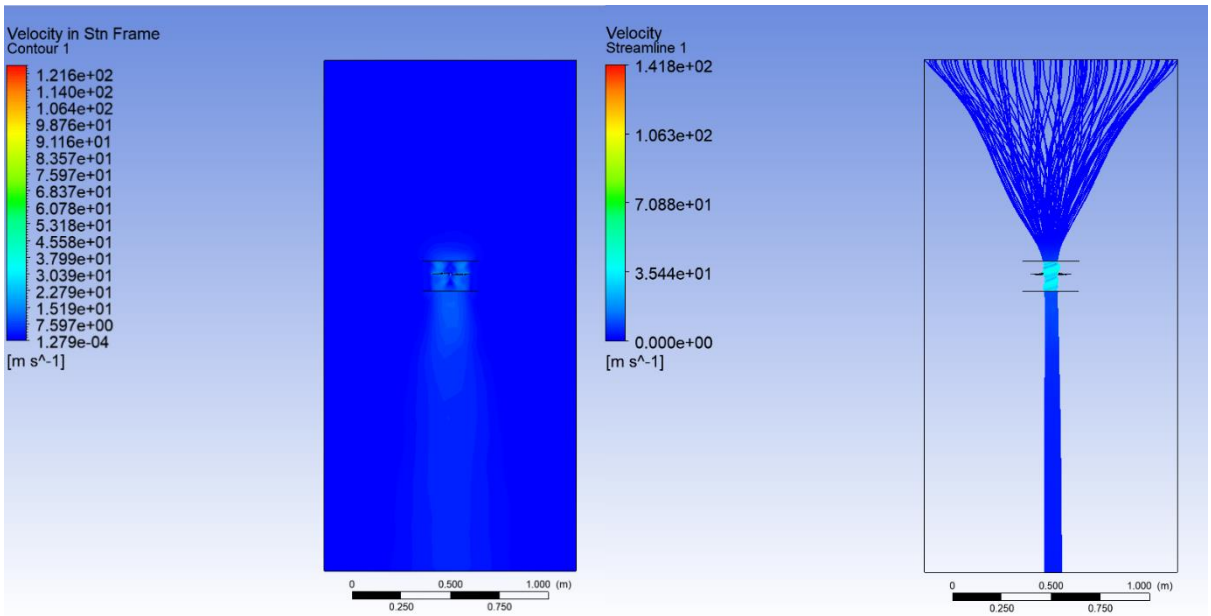

Figure 4.16: Dimpled Propeller Velocity Contour and Streamline at 9600 RPM

4.5 Dimpled and Serrated Propeller

The hybrid dimpled-serrated propeller's performance characteristics are shown in Figure 4.17. The maximum thrust remains quite higher than both base and serrated propellers, even if it is marginally less than the simply dimpled form. This suggests that the hybrid design could be appropriate for noise-sensitive UAV applications since dimples offset the propulsion penalty usually associated with trailing-edge serrations.

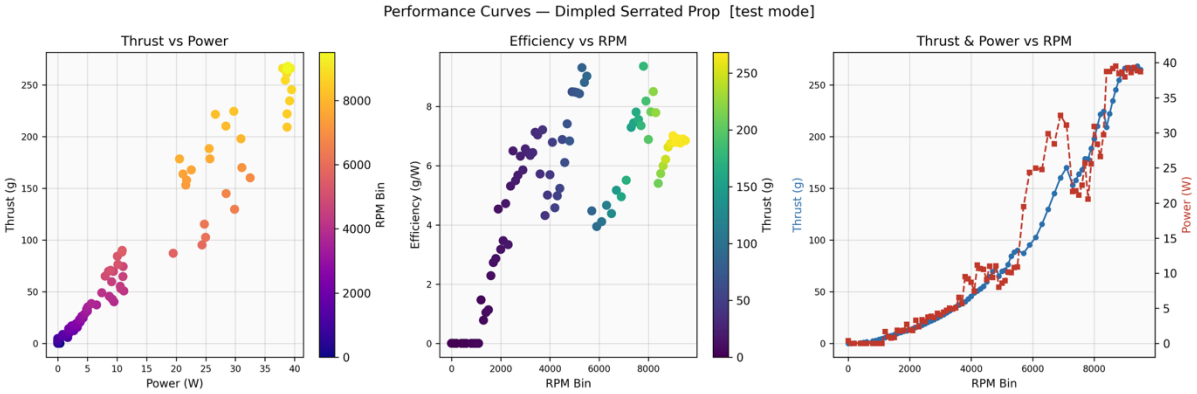

Figure 4.17: Dimpled and Serrated Propeller Performance Curves

The hybrid propeller's thrust and power consumption are compared throughout RPM in Figure 4.18. While the power curve stays relatively constrained, the thrust curve shows consistent development with RPM. The hybrid design appears to offer a workable trade-off between thrust generation and possible noise reduction based on the balance between aerodynamic performance and power efficiency.

Overall, the experimental and numerical results demonstrate that passive flow-control techniques significantly influence propeller aerodynamic behavior. Dimples primarily enhance thrust and efficiency by delaying flow separation, whereas serrations modify wake dynamics with minimal aerodynamic penalty when combined with dimples. These findings confirm the feasibility of bio-inspired surface modifications for improving UAV propeller performance.

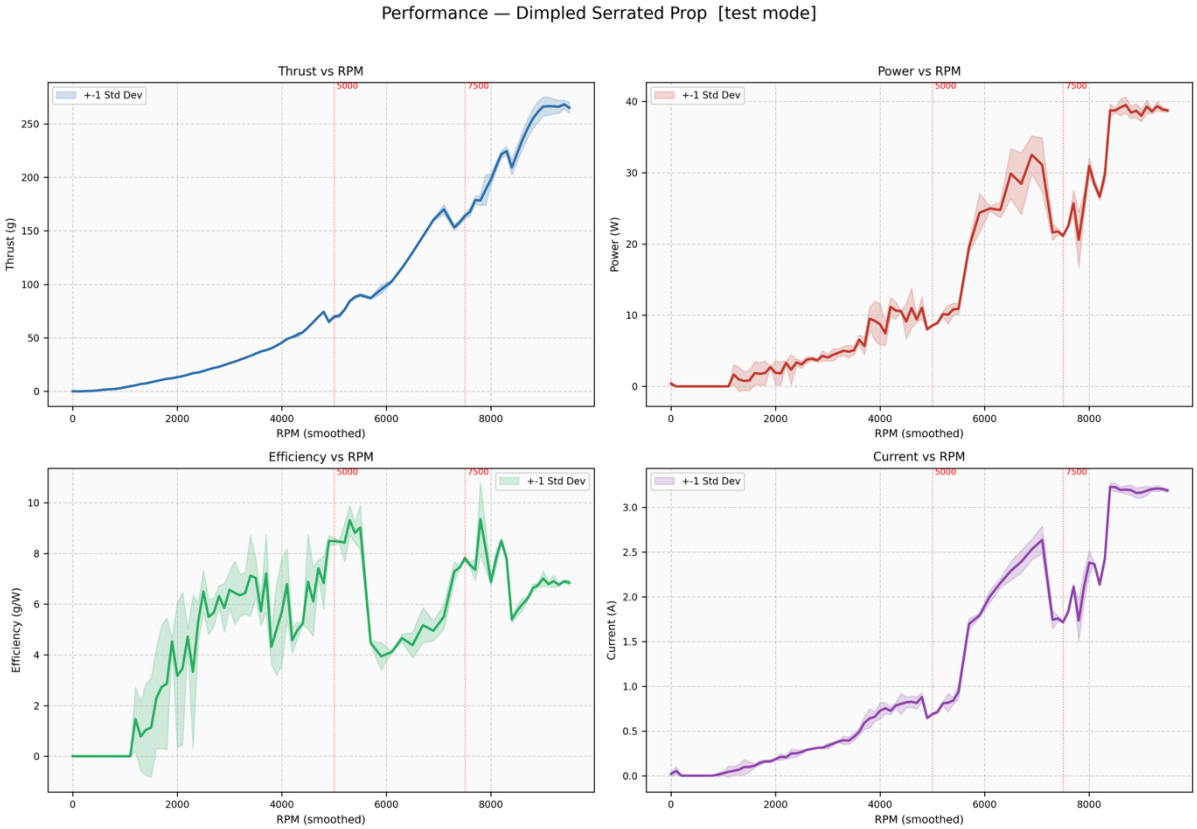

Figure 4.18: Thrust and Power comparison with RPM of Dimpled Serrated Propeller

CHAPTER FIVE:
CONCLUSION AND RECOMMENDATION

5.1 Conclusion

This study was focused on the assessment of the aerodynamic behavior of propellers with passive surface modifications like serration, dimpleds and their combined effect. In this study parametric analysis has been performed to perceive the extent of change in thrust and power consumption by propellers with surface modifications. Some of the major conclusions drawn from this study are listed below:

- Dimples on the surface change the aerodynamic behavior. When dimples are added to the surface of the propeller, their effect seems to be more pronounced at higher RPM's. Due to delayed boundary layer sepration at higher RPM's the propeller was able to generate 13.4% more thrust compared to the base propeller and 4.1% compared to dimpled-serrated propeller. Similar to other studies that has been conducted where dimples were added to the airfoil surface, it seems dimples reduce drag coefficient which inturn increase the thrust generated.
- Combination of serrations and dimples can provide the benefits of best of both world. Dimpled – Serrated propeller showed an increased in thrust of 8.99% over the base propeller at the highest RPM. Serration on the trailing edge has been shown to reduce the noise generated by the propellers but, they come with a drawback of reducing thrust. Serrated propellers, combined with the dimpled surface could be a potential solution to the thrust reduction problem.
- Surface smoothness and tip geometry could further increase the performance of the propellers. The tip geometry can have significant impact on the vortices generated and can inturn affect the noise and performance of the propeller. The resin printed propellers have a rougher surface than their market available counterparts. This can cause reduction in performance and can have a impact on the noise behavior.

Although trailing-edge serrations are widely reported to reduce aeroacoustic noise in literature, this study does not include direct acoustic measurements. Therefore, noise reduction claims are inferred based on established aerodynamic principles and previous experimental studies, and should be validated through future aeroacoustic testing.

5.2 Recommendation

This research is not absolute in itself and consists of many limitations. Some recommendation for future work are listed as below:

- This study is limited to a only aerodynamic analysis, and does not look into the aeroacoustic analysis of propellers. Hence similar study can be carried out for aeroacoustic analysis of propellers.

- While this study compares the performance of commercially available composite propeller the airfoil shape used by the composite propeller is a superior one. Passive surface modifications on these propellers can be a topic of further study.

- Serrated and Dimpled propeller with serrations pose a specific challenge to model correctly using Transition SST turbulent model. This study was only able to simulate dimpled, base and serrated propeller and further study on serrated propellers can be carried out using different turbulent models like Large Eddy Simulation (LES) or Detached Eddy Simulation (DES).

- Apart from these, study is restricted to resin printed propellers and they are unstable and prone to flutter at higher RPM. So the effect of dimples and serrations combined on the aerodynamic and aeroacoustic behavior of propellers made out of other materials can be studied.

REFERENCES

Abdullah, Abdul Qader, and Sharul Sham Dol. 2020. "Aerodynamic Investigation and Design of Dimpled Surface Airfoil for UAV Propellers." *Advances in Science and Engineering Technology International Conferences (ASET).* Abu Dhabi: AEST.

Ali, Haris, Mohammad Rasidi Rasani, Zambri Harun, and Muhammad Ashhad Shahid. n.d. "Passive flow-field control using dimples for improved aerodynamic flow over a wing."

ANYCUBIC. n.d. *14K Texture Resin.* https://store.anycubic.com/products/texture-resin.

Anyload. 2024. *How Does a Load Cell Work?* 2 9. https://www.anyload.com/how-does-a-load-cell-work/.

Arduino. n.d. *Arduino Uno Rev3.* https://store.arduino.cc/products/arduino-uno-rev3.

Bearman, P. W., and J. K. Harvey. 1993. "Control of Circular Cylinder Flow by the Use of Dimples." *Imperial College of Science, Technology and Medicine* 31 (10): 1753-1756.

Candeloro, Paolo, Daniele Ragni, and Tiziano Pagliaroli. 2024. "Experimental investigation on the application of serrated trailing edge propellers for drone noise reduction." *Aeroacoustics Conferences.* Rome, Italy: 30th AIAA/CEAS Aeroacoustics Conference (2024).

Efyian, Eben. 2024. *Understanding IR Sensors and IR LEDs: Functions, Differences, and Applications.* 08 28. https://www.electronicsforu.com/technology-trends/learn-electronics/ir-led-infrared-sensor-basics.

Elwell, J., and M. Loo. 2004. "A study of propeller tip vortex generation and the resulting acoustic signature." *The Journal of the Acoustical Society of America,* 116 (4): 2284-2291. doi:10.1121/1.1794632.

Farid, Ahmed, and Leonardo P. Chamorro. 2026. "On Bio-Inspired Strategies for Flow Control, Fluid–Structure Interaction, and Thermal Transport." *Biomimetics.*

Fikadea, Gedyon, Addisu Bekeleb, Chandraprabu Venkatachalamb, and Mohanram Parthiban. 2020. "Effects of Dimples on Aerodynamic Performance of Horizontal Axis Wind Turbine Blades." *International Research Journal of Engineering and Technology (IRJET)* 7 (1): 525-539.

Gattere, Federica, Alessandro Chiarini, and Maurizio Quadrio. 2022. "Dimples for Skin-Friction Drag Reduction: Status and Perspectives." *Fluids* (Fluids, MDPI).

GeeksforGeeks. 2023. *How to interface I2C LCD display with Arduino ?* 03 20. https://www.geeksforgeeks.org/electronics-engineering/how-to-interface-i2c-lcd-display-with-arduino/.

Gruber, Mathieu. 2012. *Airfoil noise reduction by edge treatments.* University of Southampton.

Gu, Yijuan , Fuqiang Song, Honglei Bai, Jianing Wu, Kun Liu, Bowen Nie, Liangquan Wang, Zhizhou Zhang, and Zhenbo Lu. 2024. "Numerical and experimental studies on the owl-inspired propellers with various serrated trailing edges." *Applied Acoustics* (Sciencedirect).

Howe, M. S. 1991. "AERODYNAMIC NOISE OF A SERRATED TRAILING EDGE." *Journal of Fluids and Structures* (Journal of Fluids and Structures) 5: 33-45.

Jenkins, Burton. 2001. *Wind Energy Handbook.* John Wiley & Sons Ltd. https://en.wikipedia.org/wiki/Blade_element_momentum_theory.

Jorgensen, Theodore P. 1994. *The Physics of Golf.* New York: American Institute of Physics.

Kim, D., J. Lee, C. Lee, and J. Lee. 2017. "Reduction of ship propeller noise by modifying the toroidal shape of the propeller blade tip." *Ocean Engineering* 139: 204-214. doi:10.1016/j.oceaneng.2017.05.007.

Kim, J., and W. Jeon. 2019. "CFD simulations for reducing the intensity of the propeller tip vortex by modifying the propeller geometry." *Journal of Marine Science and Technology* 24 (2): 437-450. doi:10.1007/s00773-018-0547-5.

Kumar, Sujit, Sushil Kr. Singh, Shailesh Jha, Kabilan Baskaran, K.Srinivasan, and S.Narayanan. 2024. "On the reductions of airfoil broadband noise through circular dimples." *Applied Acoustics.*

Larrabee, E. E., R. H. Liebeck, and J. Sessions. 1977. "The effects of tip geometry on the noise generated by a model propeller." *Journal of Sound and Vibration* 50 (1): 1-19. doi:10.1016/0022-460X(77)90222-6.

Li, Jing, Chunbao Liu, and Xiaoying Li. 2021. "Effects of Wavy Leading-Edge Protuberance on Hydrofoil Performance and Its Flow Mechanism." *Marine Science and Engineering.*

Microscale. 2026. *Microscale.* https://www.microscale.net/products/voltage-sensor-module.

Moreau, Danielle J., and Con J. Doolan. 2013. "On the noise reduction mechanism of a flat plate serrated trailing edge." *AIAA Journal* (The University of Adelaide) 2513-2522.

Nicola Kloet, Simon Watkins, Xu Wang, Sam Prudden, and Reece Clothier. 2017. "A preliminary investigation of the acoustic impact of unmanned aircraft systems (UAS)." International Congress on Sound and Vibration.

S, Prasath. M., and Irish Angelin. S. 2017. "Effect of Dimples on Aircraft Wing." *Global Research and Development Journal for Engineering.*

Solutions, Himalayan. n.d. *ACS712 Current Sensor Module 20A.* https://himalayansolution.com/product/acs712-current-sensor-module-20a.

Sudarsana, Putu Brahmanda , Jagmohan Singh, and Anchal Sareen. 2025. "Wake Stabilization and Force Modulation via Surface Dimples on an Airfoil at Low-Reynolds-Numbers." *arXiv:2507.23564v1* (ResearchGate) 1-9. https://arxiv.org/abs/2507.23564.

Sustainability Directory. 2025. *How Do Serrated Trailing Edges on Turbine Blades Work to Reduce Noise?* 11 20. https://energy.sustainability-directory.com/learn/how-do-serrated-trailing-edges-on-turbine-blades-work-to-reduce-noise/.

Vermeer, L.J., J.N. Sorensen, and A. Crespo. 2003. "Wind turbine wake aerodynamics." *Progress in Aerospace Science* 44. doi:10.1016/S0376-0421(03)00078-2.

Wang, D., C. Cai, R. Zha, C. Peng, X. Feng, P. Liang, K. Meng, J. Kou, T. Maeda, and Q Li. 2024. "Impact of Leading-Edge Tubercles on Airfoil Aerodynamic Performance and Flow Patterns at Different Reynolds Numbers." *Energies* 17: 5518.

Wang, Dian, Chang Cai, Rongyu Zha, Chaoyi Peng, Xuebin Feng, Pengcheng Liang, Keqilao Meng, Jianyu Kou, Takao Maeda, and Qing'an Li. 2024. "Impact of Leading-Edge Tubercles on Airfoil Aerodynamic Performance and Flow Patterns at Different Reynolds Numbers." *Energies.*

Xu, Y., H. Xie, and H. Liu. 2018. "Numerical analysis of the influence of tip vortices on propeller noise." *Journal of Marine Science and Technology* 23 (3): 504-515. doi:10.1007/s00773-017-0515-7.

Zhang, Yuan, Tao Han, Partrick Rainey, Pingling Sun, and Jun Ge. 2025. "Research on the Influence of Blade Tip Trailing-Edge Serrated Structure on Wind Turbine Noise Reduction and Performance." *Wind Energy Science Discussions.* European Academy of Wind Energy. 1-14.

ANNEX A:

PROPELLER GEOMETRY CALCULATION

Station Chord and Pitch angle calculated data
Running conditions

- $R = 0.1016$ m
- $B = 2$
- D = 0.20325 m
- RPM = 10000
- $\Omega = 1047.20$ rad/s
- $k = 449.276$
- $\frac{dT}{dr} = 449.276\, r$

Station at 75% of Radius of Propeller

Polar values from airfoil tools $\alpha = 6.5°$used (clamped to Re=50k):

$C_L = 1.0604$

$C_D = 0.0304$

$r = 0.75R = 0.07620$ m

$\frac{dT}{dr} = 34.2349$ N/m

Force, Inflow Angle, Resultant Velocity

$F = 0.99521$, $v_i = 5.4154$ m/s

$V_t = 1047.2(0.07620)(1 - 0.00661) = 79.2701$ m/s

$\phi = 3.9081°, V_r = 79.4548$ m/s

Polar (clamped): $C_L = 1.0604$, $C_D = 0.03049$

$C_T^* = 1.0604 * cos(3.9081°) - 0.03049 * sin(3.9081°) = 1.0559$

$$c = \frac{34.2349}{\frac{1}{2}(1.225)(2)(79.4548^2)(1.0559)} = 0.004196 \text{ m} = 4.20 \text{ mm}$$

$$Re = \frac{(1.225)(79.4548)(0.004196)}{1.81 \times 10^{-5}} = 22{,}562$$

$$\beta = 3.9081 + 6.5 = 10.4081°$$

$$P = 2\pi(0.07620) * \tan(10.4081°) = 0.08794 \text{ m} = 3.46 \text{ in}$$

Torque/power:

$$C_Q^* = 1.0604 * \sin(3.9081°) + 0.03049 * \cos(3.9081°) = 0.1027$$

$$\frac{dQ}{dr} = 0.25390 \text{ N/m}$$

$$\frac{dP}{dr} = 265.88 \text{ W/m}$$

Serration Calculated values at station starting from 50% to 90% of radial distance

Station (r/R)	Radius (mm)	Chord (mm)	δ (mm)	Height h (mm)	Wavelength λ (mm)	Angle ϕ (deg)
51.50%	52.27	6.18	0.307	0.615	0.461	41.11°
61.10%	62.11	5.17	0.257	0.515	0.386	41.11°
70.80%	71.94	4.41	0.219	0.439	0.329	41.11°
80.50%	81.77	3.84	0.191	0.382	0.286	41.11°
90.20%	91.6	3.39	0.169	0.337	0.253	41.11°

Dimples calculation for 40% to 90% of radial distance

Station (r/R)	Chord (c, mm)	Diameter (d, mm)	Depth (k, mm)	Sphere Radius (R, mm)
41.60%	8.24	0.165	0.0041	0.828
51.50%	6.18	0.124	0.0031	0.62
61.10%	5.17	0.103	0.0026	0.519
70.80%	4.41	0.088	0.0022	0.443
80.50%	3.84	0.077	0.0019	0.386
90.20%	3.39	0.068	0.0017	0.34

r/R	r (mm)	c (mm)	Pitch angle (Beta)	Inflow Angle (phi)	Torque (N/M)	Thrust Force	pitch (inch)	Reynolds Number (Re)
0.2	20.32	18.92631057834716	25.521681582135326	19.021681582135326	9.129293620906084	0.6925501195173285	2.3998758133393463	25513.06989
0.2241935483870968	22.77806451612903	15.763792857400473	21.65828042339796	15.15828042339796	10.23364365569311	0.8179555672565676	2.2375278967066863	24371.820276768736
0.24838709677419357	25.236129032258066	13.768333187016493	19.42370716182598	12.92370716182598	11.337993690480136	0.8911472985643478	2.201287372253681	23843.628452302073
0.2725806451612903	27.694193548387094	12.303351175763122	17.904691466772114	11.404691466772116	12.442343725267161	0.934391266	2.2133349097308104	23534.828441239206
0.2967741935483871	30.152258064516126	11.153360003209155	16.77551559811735	10.27551559811735	13.546693760054186	0.9601811440284003	2.2484516272857644	23330.281688672763
0.3209677419354839	32.61032258064516	10.215708360471451	15.887173242090213	9.387173242090213	14.651043794841213	0.975694386	2.295935878	23183.83774305357
0.3451612903225807	35.0683871	9.431830471745206	15.160939506087905	8.660939506087905	15.755393829628243	0.9850960449011619	2.3505550957317936	23073.35739355189
0.3693548387096775	37.52645161290323	8.764504612290605	14.550865372787332	8.050865372787332	16.859743864415268	0.9908285980276171	2.409515338175434	22986.853309789767
0.3935483870967742	39.98451612903226	8.188362041219152	14.028033150061933	7.528033150061933	17.96409389920229	0.9943401397520688	2.4712315691789817	22917.23379218056
0.41774193548387095	42.442580645161286	7.685257021613542	13.573125322814114	7.073125322814115	19.068443933989318	0.9964979512628487	2.534763199	22860.00882695558
0.44193548387096776	44.90064516129033	7.241744478373339	13.17259997220769	6.672599972	20.172793968776347	0.9978257898595785	2.599531894915348	22812.180189663606
0.46612903225806457	47.358709677419355	6.847589717683952	12.816582692851602	6.316582692851602	21.27714400356337	0.9986418163522028	2.6651713601431526	22771.658877531223
0.4903225806451613	49.81677419354839	6.494832625697056	12.497637199552472	5.997637199552471	22.381494038350397	0.9991397548521772	2.731443539232886	22736.938387418882
0.5145161290322581	52.27483870967742	6.177172099	12.210013440923838	5.710013440923838	23.48584407313742	0.9994370732436783	2.798190245826338	22706.90151003244
0.5387096774193548	54.732903225806446	5.889545697413707	11.949168372289769	5.449168372	24.59019410792445	0.9996036602956071	2.8653045501052787	22680.70040281546
0.5629032258064517	57.19096774193549	5.6278340168836625	11.711449650708285	5.211449650708286	25.69454414271148	0.9996786647829188	2.932713695287585	22657.67927617116
0.5870967741935484	59.649032258064516	5.388647644060076	11.493880770245703	4.993880770245702	26.798894177498504	0.9996798565845582	3.0003690746772045	22637.322966709293
0.6112903225806452	62.10709677419355	5.169170299199941	11.294011987826195	4.794011987826195	27.90324421228553	0.9996078824029068	3.0682408371457646	22619.22150645728
0.635483871	64.56516129032258	4.967041520795614	11.109816254674325	4.6098162546743255	29.007594247072554	0.9994464728061419	3.1363159868113963	22603.045616614054
0.6596774193548387	67.02322581	4.7802674407768135	10.939617877687898	4.4396178776878985	30.11194428185958	0.9991586670320137	3.204599640481693	22588.529271565374
0.6838709677419355	69.48129032258065	4.607152132322052	10.782047624226657	4.282047624226657	31.216294316646607	0.9986781272204963	3.2731199290451913	22575.45748970906
0.7080645161290322	71.93935483870966	4.446244277726591	10.63602251699102	4.136022517	32.32064435143363	0.9978933638898713	3.3419379547696444	22563.65824144132
0.7322580645161288	74.39741935483869	4.296295354021482	10.500753108303048	4.000753108303048	33.424994386220654	0.9966208408250464	3.4111655797021814	22552.99767892054
0.7564516129032257	76.85548387096773	4.156226908914731	10.375787460607372	3.8757874606073712	34.52934442100768	0.9945598015605711	3.4809962709858895	22543.379137219086
0.7806451612903227	79.31354838709679	4.025105112424306	10.261111264008562	3.761111264008563	35.63369445579472	0.9912163121414548	3.5517586348075114	22534.74658693707
0.8048387096774194	81.7716129	3.9021216899856865	10.157343291618183	3.6573432916181825	36.738044490581736	0.9857744026357838	3.6240111555699084	22527.094967233592
0.8290322580645162	84.22967741935484	3.7865812512968775	10.06610635220353	3.5661063522035303	37.84239452536877	0.976874758	3.6987154255665633	22520.492624295588
0.853225806	86.68774193548387	3.6778965855817662	9.990746387	3.4907463868764395	38.946744560155786	0.9622298741845758	3.7775678451604917	22515.12749549504
0.8774193548387098	89.14580645161291	3.5755973260645573	9.937804433	3.4378044330596014	40.05109459494282	0.9379478084384224	3.863677075445678	22511.406094152848
0.9016129032258065	91.60387096774193	3.479367874771467	9.920305111	3.4203051109933806	41.15544462972984	0.8973391885553761	3.9630793796432564	22510.18468807346
0.9258064516129032	94.06193548387095	3.389168878222812	9.966191432631815	3.4661914326318155	42.25979466451686	0.8288138061113242	4.088630500140185	22513.396576868232
0.95	96.52	3.305684307798719	10.145638565253453	3.6456385652534524	43.36414469930389	0.7120525501150318	4.272606491100499	22526.241411494495

ANNEX B:
RESULTS IN TABULAR FORM

Base Propeller 3 Sample Average Data

RPM_Bin	Thrust_g_mean	Thrust_g_std	Power_W_mean	Power_W_std	Efficiency_gW_mean	Efficiency_gW_std
0	-0.006969697	0.056731449	0.212727272727272724	0.184229465253983138	0.001041663	0.001804214
100	0.066666667	0.115470053837925116	0	0	0	0
200	0.033333333	0.057735027	0	0	0	0
300	0.199999999999999998	0.1	0	0	0	0
400	0.5	0.173205080756887677	0	0	0	0
500	0.850000000000000001	0.070710678	0	0	0	0
600	1.4	0.141421356237309556	0	0	0	0
700	1.7	0.424264068711928557	0	0	0	0
800	2.199999999999999997	0.199999999999999984	0.799999999999999999	1.385640646055101818	0.305554282412712202	0.529235541609066909
900	2.55	0.212132034355964606	0	0	0	0
1000	3.333333333333333335	0.251661147842358116	0	0	0	0
1100	4.366666666666666667	0.351188458428424606	0	0	0	0
1200	5.433333333333333334	0.404145188432737783	0	0	0	0
1300	6.75	0.070710678	0	0	0	0

1400	6.8	0.6999999999999996	2.3666666666666667	0.15275252316519466	2.889634150354893 5	0.4340800259012824
1500	7.4	1.272792206135786	0	0	0	0
1600	8.466666666666667	1.0066445913694333	0.3833333333333333	0.6639528095680696	0.5869539697653489	1.0166340973378307
1700	9.816666666666668	0.8607167555783564	0.9666666666666667	1.6743157806499147	1.2068923900262412	2.0903989387936837
1800	11.066666666666668	0.6110100926607783	0.9333333333333332	1.6165807537309522	1.3333285 71445578	2.3093928 28926971
1900	11.566666666666668	0.6110100926607783	1.8333333333333333	1.5947831618540915	2.7422534 71589501	2.3761718 32945797
2000	12.533333333333333	0.6658328118479392	2.9	0.1000000000000002	4.3287480 37242707	0.3425750632535333
2100	13.5	0.7211102550927987	2.9333333333333336	0.5131601439446885	4.6966500 19175661	0.8740376 286642507
2200	14.666666666666666	0.9504384952922179	2.4666666666666663	0.115470054	5.9639103 16182026	0.2238421 1682817318
2300	16.183333333333334	1.1094292827095098	3.2999999999999994	0.8261355820929149	5.1259907 59636036	1.4069398 48149008
2400	16.966666666666665	0.9291573243177578	3.3333333333333335	0.3055050463303893	5.1336445 05	0.7251289 657809618
2500	18	1.178982612255159	3.5666666666666664	0.25166114784235827	5.1458464 43556594	0.7302742 970652816
2600	19.416666666666668	1.2493331554606781	3.4833333 33333333	0.2254624876411448	5.6652520 730826845	0.2958430 9153987276
2700	20.633333333333333	1.0785793124908964	3.6333333333333333	1.0214368964029708	5.9243117 93903662	1.3237095 447537142
2800	21.633333333333336	1.0785793124908964	3.6	0.21794494717703353	6.1185633 42320061	0.6310055 873613634
2900	23.133333333333336	1.0785793124908964	3.8333333333333335	0.3511884584284248	6.0526991 97913569	0.3145707 101579754
3000	24.716666666666667	1.077419757259601	4.2333333 33333333	0.7588368291888141	6.0368189 34772152	1.3158638 683892643
3100	25.766666666666667	1.0408329997330663	4.1333333 33333334	0.4041451884327375	6.2846692 53881432	0.7948076 707480136
3200	27.349999999999998	1.0816653826391975	4.0666666 66666666	0.1040832999733062	6.8079781 06366441	0.2357978 608162047

3300	29.516666666666666	1.0692676621563626	5.266666666666667	0.5033222956847174	5.866495435	1.058939538186995
3400	31.216666666666667	1.1622535581074107	5.716666666666666	0.6006940430313366	5.514835303209799	0.7740935403858977
3500	32.533333333333334	1.3363507523600748	5.116666666666666	0.3403429642777024	6.515626734266932	0.41932371424608506
3600	34.433333333333333	1.2503332889007361	5.383333333333333	0.7522189397597838	6.540184319961774	0.7021741696752021
3700	35.866666666666667	1.2096831541082684	7.533333333333334	1.0016652800877817	4.818504503264697	0.6734645577792944
3800	37.183333333333333	1.2413030787576915	8.233333333333333	0.907377173	4.562915219256148	0.6087777036165612
3900	38.533333333333333	0.47258156262526146	8.733333333333333	0.9865765724632497	4.448422197162103	0.48090192452868374
4000	38.800000000000004	1.0392304845413252	9.433333333333332	0.6806859285554039	4.131945418	0.3926564538945392
4100	39.866666666666667	1.550268793897796	9.766666666666667	0.6110100926607798	4.098473349338536	0.40328527630199595
4200	40.866666666666667	1.6441816606851358	10.933333333333332	1.2503332889007368	3.759589071	0.2878839019528111
4300	43.3	1.6970562748477156	10.6	4.1012193308819755	4.448864741127754	1.8813969375161053
4400	46.466666666666667	1.6802777548171433	9.700000000000001	1.081665382639196	4.824386363197049	0.4725544239164541
4600	51.9	1.2165525060596454	12.299999999999999	1.6643316977093243	4.282166407226637	0.6960522669120881
4700	44.383333333333333	11.418442684242601	8.566666666666668	1.2583057392117918	5.341819903183598	2.0113199995804676
4800	42.34621212121212	3.676556519008725	8.303409091	0.10863422401848886	5.294589321004158	0.4930245058665747
4900	51.809464285714284	2.2460045804172153	9.007678571428572	0.3412661654240936	5.938758934047179	0.26448713838974347
5000	58.44145536606697	3.5046331779292386	8.15484742	0.2869330168545831 7	7.484980320073835	0.4267182303297425
5100	62.932054673721346	2.983287494531773	8.383383723859914	0.285807979	7.936393922630411	0.4145531840053973
5200	66.79444444444444	2.3168515114106656	9.605555555555556	1.1619348486867027	7.596893496609293	1.0490114833815691

5300	72.19444444444444	2.4228273963682563	10.422222222222222	0.7934337	7.420039402263401	0.48772695653317305
5400	78.43444444444445	1.6569125683810948	9.142222222222221	0.47259723671235004	8.669288069875572	0.5073793901520618
5500	80.75622895622895	2.861494992092373	9.733333333333333	0.19757482803276427	9.018981289309314	0.5478253976600252
5600	74.19999999999999	1.5556349186104015	20	0	3.709998145000927 4	0.077781707
5800	82.05000000000001	1.6263455967290623	21.5	0.282842712	3.817105166795172 5	0.12585975429342983
6000	91.4	1.8384776310850346	26.4	1.1313708498984734	3.463808428752302 3	0.078802025
6200	102.15	2.050609665440987	25.75	1.2020815280171329	3.973176880927482 6	0.2651141572973615
6500	107.85	6.151828996	27.85	0.070710678	3.872822930477863 4	0.23072447485550363
6600	119.80000000000001	2.262741699796959	27.45	4.596194077712559	4.433344232500032	0.824744771
6900	128.8	1.979898987322311	31.599999999999998	4.525483399593903	4.113646074323366	0.5264662268724819
7000	143.85	1.9091883092036703	30.299999999999997	0.8485281374238578	4.750268117896381	0.19603704644144346
7200	152.29999999999998	6.200000000000002	29.766666666666666	2.3288051299611428	5.140606321071107	0.5059825011638577
7300	129.58869047619046	5.7601707778030145	18.78154761904762	0.3627081269756023 4	6.961367717703471	0.28704061962168037
7400	134.67673992673994	5.507328343145096	20.216849816849816	1.1033434019567014	6.811639509504519	0.25885161930633094
7500	137.4599328938173	5.493982860199082	19.812573090015054	0.6136714686201924	6.983582857126688	0.065388692
7600	139.06965461062236	5.438341495979657	20.855265558813944	0.4636615201937074 3	6.791285704587328	0.22599492534398283
7700	150.13333333333333	4.9006589692951925	24.141666666666666	1.640185456993608	6.637500208242788	0.7496003618301961

7800	148.65833333333333	9.768902616636797	20.658333333333335	3.111504191437534	7.535099495443025	0.5716980607949327
7900	155.90833333333333	5.324139210551645	25.341666666666665	0.38432841858667227	6.724190563121243	0.22410155215554736
8000	170.55277777777778	9.204551762478607	29.644444444444446	1.898214316823206	6.178049764399147	0.3834551658761472
8100	180.6783333333333	2.581503115	25.921666666666667	1.738507501661506	7.353171460538047	0.49437303967261337
8200	186.56333333333336	6.544542255447149	25.813333333333333	3.624711482771191	7.461826218505454	0.9529500961813405
8300	196.63809523809525	5.032026680871917	28.323809523809526	0.763629001348612	7.145374871222857	0.20085871784518874
8400	181.53333333333333	3.3560889936551623	36.5	1.058300524425836	4.975042452194236	0.10087240165055658
8500	191.29999999999998	6.221736092120891	36.46666666666667	0.45092497528229036	5.247380105	0.2189380909681804
8600	200.70000000000002	5.534437640808686	36.36666666666667	0.32145502536643233	5.518747598686740 5	0.1410090066632834
8700	209.5	2.6457513110645907	35.9	0.953939201	5.837130248492513	0.084009404
8800	219.56666666666667	3.629508690351002	35.71666666666667	0.8129165598838147	6.149392051626115	0.1672183656370769
8900	227.6833333333333	3.6763886265373817	36.25	0.3122498999199209	6.282620646348715 5	0.15068798968126362
9000	230.61666666666667	3.9913448026114526	35.583333333333336	1.249333155460680 1	6.484522034864214	0.14571431408819197
9100	230.71666666666667	5.507898369109988	36.68888888888889	0.153960071783899 67	6.289496818013746	0.1238876723648659
9200	230.36666666666667	6.400347212803715	36.19999999999996	0.41633319989322803	6.370037788669808 5	0.15688996060556754
9300	230.54777777777778	6.401524413357711	36.16555555555556	0.8584244827546571	6.377667752087248	0.17621983402759006
9400	231.8584986772487	5.472618889660521	36.37972883597883	0.566604766	6.376388721479132	0.077534985
9500	228.11450353035684	3.8265986105191145	35.80567710975816	0.5279037343386274	6.374719403166572	0.05199077

Dimpled Propeller 3 Sample Average Data

RPM_Bin	Thrust_g_mean	Thrust_g_std	Power_W_mean	Power_W_std	Efficiency_gW_mean	Efficiency_gW_std
0	0.008754209	0.16885714908041377	0.30404040404040406	0.26352023449513046	9.161955214530167e-05	0.005429002
100	-0.033333333	0.15275252316519466	0	0	0	0
200	-0.066666667	0.11547005383792516	0	0	0	0
300	0.100000000000000002	0.1	0	0	0	0
400	0.300000000000000004	0.14142135623730951	0	0	0	0
500	0.7333333333333334	0.15275252316519475	0.7666666666666666	1.3279056191361391	0.13043421550341086	0.22591868829729578
600	1.2999999999999998	0.14142135623730956	0	0	0	0
700	1.9666666666666668	0.25166114784235850	0.8666666666666667	1.501110699893027	0.25640927022075555	0.4441138835540061
800	2.4000000000000004	0.42426406871192873	1.25	1.7677669529663689	0.41999832	0.5939673203274186
900	3.1333333333333333	0.7023769168568493	0	0	0	0
1000	3.9000000000000004	0.7071067811865477	1.35	1.9091883092036785	0.8148117969933445	1.1523178940895809
1100	4.8	0.2828427124746193	0	0	0	0
1200	6.0666666666666666	0.30550504633038950	0	0	0	0
1300	7.4333333333333334	0.23094010767585058	0.8666666666666667	1.501110699893027	0.9358938363057577	1.6210156749721225
1400	8.6333333333333333	0.5033222956847165	0	0	0	0
1500	9.5333333333333333	0.15275252316519375	1.7666666666666666	1.569500982265807	2.4178649545288344	2.143894409414971

1600	10.866666666666667	0.23094010767584988	2.966666666666667	0.4725815626252607	3.716104319270089	0.501965034
1700	12.133333333333335	0.28867513459481275	1.0999999999999999	1.905255888325765	1.191915580053798	2.0644583429861076
1800	13.366666666666667	0.32145502536643156	0.7666666666666666	1.3279056191361391	1.9565132325511627	3.3887803244594363
1900	14.366666666666667	0.37859389	2.066666666666667	1.7925772879665003	3.123601007266513	2.7164543938961954
2000	15.366666666666667	0.6506407098647715	1.6666666666666667	1.446835627614047	4.092932321523712	3.5446127141470645
2100	17.099999999999998	0.7262919523166961	3.0833333333333335	0.2362907813126305	5.596702639192181	0.6349481332871816
2200	18.599999999999998	0.529150262	2.6	0.36055512754639896	7.242483542170654	0.9977734163295651
2300	19.633333333333333	0.5859465277082324	3.0666666666666664	0.15275252316519494	6.407480443339757	0.18953058111505233
2400	20.966666666666665	0.6110100926607804	3.5666666666666664	0.076376262	6.009453008544308	0.2613590138195541
2500	22.833333333333332	0.7023769168568484	3.8333333333333335	0.5131601439446887	6.016376030123357	0.6982019568893755
2600	24.283333333333333	0.9878427675158309	3.4833333333333333	0.5346338310781813	7.120637834	1.1586566893647028
2700	26.066666666666666	1.0785793124908976	4.516666666666667	0.8836477427874375	5.945658370642043	1.1963864722723936
2800	27.433333333333337	1.0408329997330663	4.600000000000005	0.6082762530298219	6.042701106205338	0.7130163178941678
2900	29.575	1.4495689014324253	3.95	0.7778174593052025	8.095810049497297	1.2786802560075958
3000	31.5	1.4142135623730951	4.125	0.4596194077712552	7.734371859655885 5	0.4128411942251078
3100	32.900000000000006	1.1313708498984745	5.050000000000001	0.35355339059327473	6.633570256709447	0.5476520098823462
3200	35	0.9192388155425097	5.324999999999999	0.7424621202458744	7.081981794007651 5	1.6910810924247393
3300	37.6	0.9192388155425097	5	1.2020815280171302	7.815457301999668	1.9908962553658427
3400	39.333333333333336	1.0128343069492332	4.716666666666666	2.0508128469788103	9.959257689974178	5.168036431249674
3500	41.46666666666667	1.3012814197295397	5.233333333333333	0.4509249752822896	8.068311557970523	0.4864528079973909

3600	43.666666666666664	1.0128343069492298	7.55	1.130265455545731	5.922510549836349	0.8872409107167353
3700	45.36666666666667	0.986576572	6.683333333333333	2.765110004	7.654245110495509	3.1581036707712125
3800	47	1.6370705543744861	7.933333333333334	1.2013880860626736	6.022063126368202	0.9744548704121327
3900	49.71666666666667	1.3823289526495959	9.133333333333333	0.9712534856222302	5.483413077755064	0.4382465094385944
4000	53.166666666666664	1.0263202878893771	11.4	1.7349351572897467	4.732282289115201	0.6810331493994466
4100	56.9	1.2727922061357835	8.45	0.9192388155425113	6.765559673425454	0.5853688758410951
4200	57.2	1.272792206135786	11.100000000000001	2.545584412	5.278814704531197	1.095933807
4300	60.199999999999996	2.2271057451320075	13.466666666666667	1.9553345834749956	4.523270533643624	0.5726270244136755
4400	64.76666666666667	2.631222783	11.299999999999999	1.4177446878757827	5.770548422474353	0.4664622964040415
4500	69.76666666666667	2.8290163190291637	10.233333333333333	2.2810816147900828	7.026788140788464	1.4127308261782872
4600	73.44999999999999	1.6263455967290623	13.3	0.2828427124746199	5.525101864983609 4	0.2397803053508287
4700	78.43333333333334	1.3316656236958857	12.799999999999999	0.6928203230275507	6.137116400122392	0.2724141143290528
4800	80.899999999999999	1.410673597966594	13.466666666666667	2.610236260060251	6.155415949	1.1621709912318339
4900	73.39484126984127	1.458737229459347	8.943730159	0.5988272899633408	8.537966870083835	0.3735861162604912 6
5000	80.31355591781708	2.0006216714154275	9.567576791417613	0.1079932794199754	8.746524869468672	0.2879776193078123 5
5100	80.78665205212519	2.2852158589006346	9.990244793569602	1.3328624264076505	8.593134835	1.0157553290435966
5200	87.86111111111113	0.9788504217438636	10.444444444444445	0.6351581896865736	8.841213899168906	0.6894091933
5300	94.37904761904763	1.2064599364385413	11.030476190476191	0.6494288437767858	9.024093560235093	0.5690010889400315
5400	98.60062271	2.1206367120288303	11.94959706959707	0.5432608537255359	8.688421582516552	0.6879419961900306
5500	95.73333333333333	7.691607980996775	18.116666666666667	7.840652608892537	6.626837817670512	2.9821296166745923
5700	96.3	1.7000000000000028	25.166666666666668	2.7537852736430515	3.859522250572819	0.4537467137348300 5
5900	106.13333333333333	1.625833119767626	25.033333333333333	1.0785793124908958	4.246755295880844 5	0.2484379188514464 5
6100	118.10000000000001	1.5716233645501738	28.2	1	4.190424186686669	0.1109832573103545 8

6300	132.35000000000002	2.192031021678303	32.55	0.9192388155425123	4.066721754790697	0.047504055062855155
6500	151.65	8.131727983645296	32.75	2.4748737341529163	4.634383806431177	0.10191712225049236
7300	166.3955687830688	1.9366195844788339	23.195833333333336	0.785049096	7.221819324375812	0.26351788491212286
7400	170.98982683982683	2.3489461014910615	23.974242424242423	0.33452615	7.214285521716856	0.19901033144634564
7500	181.14937777777777	4.904503346736347	24.674555555555557	0.15608013729895015	7.387627789180329	0.17091388136341948
7600	185.1728021978022	3.2609742563336686	25.160347985347986	0.537739924	7.428339453588353	0.3058582332105579
7700	179.89999999999998	2.4041630560342755	31.616666666666667	6.198969448402066	6.040505335010511	1.542209379155191
7800	186.92222222222222	3.2069946702192627	34.21111111111111	7.477769523	5.787538754570076	1.588593113066742
7900	194.9	0.28284271247460296	37.1	13.293607486307096	6.008470341489794	2.563647199108136
8000	197.46666666666667	6.277207447052669	46.633333333333326	1.443375672974065	4.239659930420128	0.2571145508791065
8100	205.76666666666665	4.488132499529533	44.43333333333334	1.137248140615467	4.634509694715519	0.213608545563589 46
8300	217.79999999999998	4.107310556	44.56666666666666	3.3291640592396954	4.909623227443663	0.4545255061238017
8400	228.53333333333333	7.657893531078477	43.4	1.8248287590894683	5.274507113	0.3485700422737081
8500	239.4333333333333	6.304231383232472	44.4	0.7999999999999998	5.393026281	0.12983122008142808
8600	253.86666666666667	6.819335255971319	43.96666666666667	0.5507570547286039	5.775528238807318	0.1452278272728203
8700	264.26666666666665	7.111493045298803	45.5	0.754983444	5.808027754652545	0.12039749108092769
8800	274.28333333333336	6.711246779349802	44.683333333333334	0.975106832	6.142219391371984 5	0.22083438437555525
8900	281.1666666666667	7.242639942267805	44.5	1.0392304845413263	6.324474368972548	0.062683054
9000	283.9166666666667	4.990323970779221 5	44.11666666666667	1.079737622449704	6.438386427	0.053633041
9100	283.8972222222222	5.3471197681382385	44.54166666666664	2.1287222301966366	6.382793222	0.24797304313989568
9200	283.38000000000005	5.757534194427316	44.68333333333334	0.675154303	6.348760448 9829295	0.21511622248869247

9300	282.72200854700856	4.348191997	44.779120879120875	0.9888996850949168	6.3199179885530405	0.10787152974878862
9400	282.7224215204835	1.7178750807262233	44.175210577536156	0.458041063	6.408156247961325	0.028351173

Serrated Prop 3 Sample Average Data

RPM_Bin	Thrust_g_mean	Thrust_g_std	Power_W_mean	Power_W_std	Efficiency_gW_mean	Efficiency_gW_std
0	0	0	0	0	0	0
100	0	0	0	0	0	0
200	0	0	0	0	0	0
300	0.1666666666666666	0.057735027	0	0	0	0
400	0.4000000000000001	0	0	0	0	0
500	0.8	0	0	0	0	0
600	1.15	0.3535533905932736	0	0	0	0
700	1.45	0.070710678	0	0	0	0
800	2.1333333333333333	0.057735027	0	0	0	0
900	2.5333333333333333	0.057735027	0	0	0	0
1000	3.4666666666666667	0.057735027	0	0	0	0
1100	4.45	0.070710678	0	0	0	0
1200	5.2333333333333333	0.5507570547286103	0	0	0	0
1300	6.3333333333333333	0.550757055	0	0	0	0
1500	7.3999999999999995	0.26457513110645875	1.25	1.2031209415515964	1.506166798	1.500031856223925
1600	8.5666666666666666	0.5507570547286098	1.8333333333333333	1.588500340992514	2.1238899716718476	1.8526387173596184
1700	9.7166666666666667	0.4536885862938725	0.3833333333333333	0.6639528095680696	0.7318808758802499	1.2676548 62112604
1800	10.833333333333334	0.461880215	2.2666666666666666	2.0033305601755624	2.2070108704421147	1.950605208072916
1900	11.549999999999999	0.049999999999998934	2.6	1.212435565298214	3.1180452152076086	0.6617202083169407
2000	12.5	0.1	2.0666666666666667	1.8339392937971892	2.7460225833853857	2.440361195729561

2100	13.3666666666666667	0.1527525231651945	1.5999999999999999	1.3892443989449805	3.7020135 01967832	3.2176434 80539966
2200	14.2333333 33333334	0.11547005 383792602	2.8000000 000000003	0.2645751 3110645886	5.1169929 77575716	0.5348237 894074586
2300	15.1833333 33333332	0.14433756 729740746	2.4	2.0784609 69082653	2.9030097 52742085	2.5191715 72672759
2400	16.2333333 33333334	0.057735027	2.9833333 33333334	1.5267066 952539818	3.9732813 308667563	1.4625408 49844852
2500	17.2666666 66666666	0.15275252 316519508	3	0.9165151 389911679	6.1039815 50107936	1.7264950 49537209
2600	18.6333333 33333333	0.17559422 92142138	3.7166666 666666663	0.3055050 463303892	5.2445637 62904916	0.671123731
2700	20.0999999 99999998	0.2000000 00000024	4.0333333 33333333	0.2516611 478423583	4.9974477 637687125	0.3375290 639577365
2800	20.7666666 66666666	0.15275252 316519275	3.9166666 666666665	0.8751190 395216717	5.5092255 64001185	1.3044188 46748349
2900	22.3166666 66666666	0.10408329 997330641	3.85	0.4444097 208657792 3	5.8706434 91456943	0.6509636 992182348
3000	24.05	0.21794494 717703433	4.75	0.6144102 863722256	5.2398067 53667869	0.8395134 569285867
3100	25.1833333 33333334	0.20207259 421636878	4.5333333 33333334	0.1527525 231651947 2	5.6123881 19902918	0.2786140 795955852 6
3200	26.8333333 33333332	0.16072751 26832158	4.1499999 999999995	0.2783882 181415014	6.6379764 15298187	0.2562925 495958101
3300	28.8	0.37749172 17635376	5.3	0.7053367 989832938	5.5971498 25	0.8430047 975082374
3400	30.45	0.47696960 07084745	5.0833333 33333333	1.2271240 089466644	6.4212536 55	1.4872151 352009113
3500	31.7833333 3333333	0.35472994 42298805	4.8833333 33333334	0.8607167 555783568	6.8801639 25	1.1476308 511269577
3600	33.75	0.27838821 814149933	5.8166666 66666666	1.1557825 631723877	6.0047028 85183427	1.1786012 281391638
3700	35.4166666 66666664	0.27537852 73643045	7.2666666 66666667	0.7505553 499465135	4.9710205 768330695	0.6187098 625427325
3800	36.3666666 6666667	0.86216781 04251669	7.7666666 66666667	1.6441816 60685136	4.8607770 42950904	1.2700710 369631414
3900	38.15	1.06418983 26896415	8.2333333 33333333	1.7616280 348965085	4.7828025 86925417	1.0262741 766095012
4000	39.8333333 33333336	1.19303534 45448838	9.4333333 33333332	0.6658328 118479403	4.2423805 23346991	0.4225089 566075341
4100	41.2666666 6666667	1.59478316 1854093	10.5	2.3065125 189341584	4.0512225 70088449	0.8294517 632675962

4200	42.56666666666666	1.4294521094927661	9.633333333333333	2.289832599412746	4.5555946040756945	0.864066382
4400	46.1	0.7549834435270723	8.366666666666667	0.30550504633038834	5.515995247569202	0.2581293459215844 3
4500	49.96666666666666	0.7637626158259743	9.566666666666666	2.0502032419575706	5.409276246030056	1.3063164237607028
4600	54.23333333333333	0.7094598884597579	11.966666666666667	1.9035055380358978	4.618373447184274	0.8179783421844552
4700	58.6	0.7211102550927948	10.700000000000001	1.442220510185596	5.544174933726165	0.7518114252588671
4800	48.28472222222222	3.3671625391143234	8.434090909090909	0.420319389	5.996232918513878	0.6087819614550295
4900	51.764040404040404	1.7360876964444933	8.247272727272728	0.7228318963723337	6.535908981574598	0.46991930582762204
5000	56.685439583333334	0.8682241841813672	8.248318750000001	0.12758860018997412	7.196540301071908 5	0.1723686971748542 9
5100	61.588459770114945	1.2934826870707952	8.366712643678161	0.550216515	7.884956731093847 5	0.5358226760026294
5200	67.511666666666667	1.5081970472499 04	10.256666666666666	1.072617514929404 8	7.225391215015083	0.7797702331816475
5300	73.322222222222224	2.1190494025317 98	9.271111111	0.9794858817729805	8.954690227	0.4194779876299497
5400	79.13293651	0.8086833288620715	8.956349206349207	0.2853602303638656	9.502307725202542	0.4946660141421232 4
5500	81.225462962962 96	1.2441532500744343	10.47638888888889	0.2986175709895583	8.796498807386072	0.6187438988836637
5700	74.033333333333333	0.5859465277082359	18.8	0.8000000000000007	3.942037267383423	0.1462889052783119 3
5900	82.933333333333334	0.8326663997864544	21.933333333333334	1.8876793513023697	3.798601248299452	0.3078812732833235
7300	133.96074074074076	1.8151098777519747	17.979629629629628	0.3343656853246658	7.543572350391762	0.2757717716296603
7400	137.9356060606061	2.2476368827000943	20.288282828282828	0.4691414440453627	6.8432608611503545	0.093541471
7500	143.59112595972763	2.238760301	19.912498189193105	0.5498249617848869	7.2717611794987675	0.095796942
7600	145.28346894662207	1.1416605920095233	20.31315747	0.28065579290687986	7.221615145563544	0.072849151
7700	145.78333333333333	2.531962348324574	18.716666666666665	4.250392138771827	8.060642506981504	1.4440948266980511

7800	150.25	0.6363961030678768	19.1	0.7071067811865476	7.9183604858853425	0.26697095643267693
7900	152.85	2.616295090390218	28.95	13.50573952066306	6.070566399260192	3.038422983722926
8800	231.20000000000002	2.621068484416224	37.06666666666667	0.15275252316519608	6.237388872098319	0.063046077
8900	237.03333333333333	6.068223243531289	35.53333333333333	0.8020806277010616	6.677999204	0.3233545645744619
9000	241.41666666666666	5.182261411134467	36.41666666666664	0.5838093296045637	6.631688802729784	0.19023433106435697
9100	243.25	4.262335040796297	36.45555555555556	0.2678791878053599	6.673899468004201	0.099747211
9200	243.4611111111111	3.594143899507968	36.73333333333333	1.484362938547491	6.633922555938992	0.1832828070929883
9300	243.44833333333335	3.052623188887434	36.81333333333333	0.29437787507442453	6.619089330168582	0.097974816
9400	242.23714285714286	2.807245727	36.53142857142857	0.31819644811317377	6.638172666445563	0.022751591
9500	242.10757007270263	1.002037824008073 8	36.26302672536104	0.3632966146671883	6.681879587890059	0.059704334
9600	237.6637478	3.564618556513641 7	35.92185828877005	0.1972903545904192	6.622372649260278	0.1333488984749871

Dimpled and Serrated Propeller

RPM_Bin	Thrust_g_mean	Thrust_g_std	Power_W_mean	Power_W_std	Efficiency_gW_mean	Efficiency_gW_std
0	0.010606060606060605	0.066546034	0.3745454545454545	0.3399708300564273	0.002529043	0.004380431
100	-0.033333333	0.057735027	0	0	0	0
200	0.100000000000000 02	0.1	0	0	0	0
400	0.466666666666666 6	0.057735027	0	0	0	0

500	0.9333333333333332	0.11547005383792512	0	0	0	0
600	1.5666666666666667	0.15275252316519464	0	0	0	0
800	2.2	0.14142135623730917	0	0	0	0
900	2.8000000000000003	0.19999999999999984	0	0	0	0
1000	3.7999999999999994	0.29999999999999998	0	0	0	0
1100	4.6999999999999999	0.14142135623730995	0	0	0	0
1200	5.6666666666666667	0.3511884584284246	1.6666666666666667	1.446835627614047	1.4668744641234144	1.2703758181146347
1300	6.8333333333333333	0.25166114784235855	0.9666666666666667	1.6743157806499147	0.7816065002074706	1.3537821698854333
1400	7.3999999999999995	0.19999999999999994	0.7666666666666666	1.3279056191361391	1.0434737240272869	1.8073495063783662
1500	8.5666666666666666	0.11547005383792475	0.8333333333333334	1.4433756729740645	1.1333288000181332	1.962983063312474
1600	9.6333333333333333	0.057735027	1.8666666666666665	1.6165807537309522	2.285706122478134	1.9794795676516894
1700	10.700000000000001	0.10000000000000009	1.7666666666666666	1.569500982265807	2.728491747294379	2.4282600242680332
1800	11.700000000000001	0.10000000000000009	1.8666666666666665	1.6921386861996073	2.8629667114946677	2.590066443006417
1900	12.233333333333334	0.15275252316519597	2.6999999999999997	0.1	4.534103380268202	0.13952425780315994
2000	13.233333333333334	0.15275252316519597	1.8999999999999997	1.705872210923198	3.172968115383013	2.835347965128128
2100	14.200000000000001	0.20000000000000107	1.8333333333333333	1.588500340992514	3.467359518723068	3.003385393610330 7
2200	15.516666666666666	0.35472994422987897	3.3000000000000003	0.2645751311064591	4.720464873301760 5	0.2998227340062609 7
2300	16.983333333333333	0.3818813079129866	2.35	2.114828598	3.332901808122904	3.0167908227658584

2400	17.633333333333333	0.25166114784235816	3.3666666666666667	0.47258156262526074	5.309385537374457	0.770449129
2500	18.983333333333334	0.43108390521258344	3.0833333333333335	0.5057996968497839	6.498710557045108	0.8294074106616668
2600	20.5	0.4582575694955835	3.7666666666666667	0.4041451884327376	5.493734832105865	0.6928109374989898
2700	21.833333333333332	0.23094010767585024	3.8666666666666667	0.32145502536643167	5.677308042977615	0.5555763556290436
2800	22.983333333333334	0.24664414311581245	3.6666666666666665	0.2516611478423584	6.319602009526366	0.4159754447863195 4
2900	24.583333333333332	0.25658007197234406	4.2833333333333333	0.742181469	5.854806181963752 5	0.9580979639825268
3000	26.233333333333334	0.2565800719723443	4.05	0.4444097208657793	6.566356898937191	0.7225422816356989
3100	27.733333333333334	0.33291640592397126	4.4333333333333334	0.8621678104251712	6.445359427366623	1.2547170313369767
3200	29.583333333333332	0.25658007197234406	4.7166666666666666	0.5795112883571243	6.345957533554743	0.8283228487640046
3300	31.3	0.25	5	0.6383572667401856	6.441094748468583	0.8252004281970622
3400	33.166666666666664	0.40414518843273756	4.8833333333333334	0.8751190395216717	7.125991239718981 5	1.6036196871351398
3500	35.233333333333334	0.4509249752822922	5.0666666666666666	0.56199051	7.036883071275668	0.7743463459648573
3600	37.199999999999996	0.26457513110645914	6.55	0.6383572667401853	5.718804715855228	0.564996319
3700	38.483333333333334	0.10408329997330953	5.6666666666666667	1.2342339054382407	7.211161531066128	1.5306972597516086
3800	40.216666666666667	0.25658007197234467	9.5	1.5716233645501712	4.315378499	0.6836664435877876
3900	42.766666666666667	0.4509249752822922	9.2000000000000001	2.740437921208945	5.005539209581705	1.8071882593650854
4000	45.533333333333333	0.4041451884327358	8.7000000000000001	2.882707061079915	5.692692239	2.0994433494040687

4100	48.93333333333334	0.3785938897200218	7.433333333333334	1.6653327995729068	6.789486448323632	1.3949300527522912
4200	50.7	0.42426406871193206	11.149999999999999	1.3435028842544399	4.578022087997217	0.5135710022406149
4300	52.85	2.4748737341529163	10.65	1.2020815280171302	4.981051176003562	0.32983592265443645
4400	55.2	0	10.55	0.070710678	5.2323400536902565	0.03506938
4500	59.63333333333333	0.3785938897200147	9.1	2.4637369989509836	6.8823941335252306	1.853726564326237
4600	64.63333333333334	0.40414518843273234	11	2.787471973	6.105911330279453	1.3673379214587935
4700	69.60000000000001	0.3999999999999968	9.4	0.3605551275463995	7.412459814760424	0.32154301585634726
4800	74.33333333333333	0.35118845842842455	11.033333333333333	1.5534906930308806	6.833713506036875	1.029020352515252
4900	64.99532828282828	1.7197954322588767	8.006565656565657	0.10930464471648119	8.494095834942021	0.20717679464657685
5000	71.2060558509329	1.456065365797393	8.566510989	0.14476320093061776	8.486052313	0.13467969394253568
5100	70.68974358974359	1.8763135107172104	8.925446775446774	0.22229857456205254	8.466447738088762	0.071129184
5200	76.33222222222223	1.3814659417257313	10.151111111111112	0.3766863318367054	8.428623254763432	0.7565077809590117
5300	84.30761904761904	1.1156560560379396	10.066666666666666	1.3273030299571136	9.308955013272367	0.581982428
5400	88.21657407407407	1.597738571931813	10.819537037037037	0.8610914125584427	8.811926325764967	0.3951582740477929
5500	89.93809523809523	1.6911735650757116	10.877248677248678	0.7512722615123946	9.022647559126057	0.8648798270263526
5700	87.16666666666667	1.4571661996262921	19.5	0.7000000000000005	4.472106045633952	0.084800076
5900	95.2	4.036087214122112	24.366666666666664	2.750151510977774	3.944862974877985	0.5388557366405127
6100	102.600000000000001	1.3076696830621966	24.966666666666667	0.3511884584284232	4.109653676769003	0.039406391248149465
6300	115.333333333333333	1.2741009902410894	24.766666666666666	1.0969655114602899	4.661362721337043	0.15579743534741045
6500	129.733333333333335	1.2096831541082578	29.866666666666664	3.5019042438884079	4.382594902651708	0.49925943910431664
6700	144.96666666666667	1.1239810200058225	28.433333333333334	4.336281049	5.169350854292328	0.6984641956347682

6900	160.2000000000000002	1.2999999999999936	32.5	2.6907248094147427	4.950475183756015	0.3855925809715686
7100	170.0666666666666666	4.593836450433711	31.099999999999998	3.7643060449437447	5.507909131211259	0.4900185235510305
7300	153.1747138047138	2.524691999069918	21.617643097643096	1.124872382578295	7.292659095168301	0.3810385057540998
7400	157.9085275835275 6	2.662122551784724	21.75928515928516	0.4445040127760675	7.445038314475371	0.053559899
7500	163.8407265560258 8	2.4155899209973275	21.148274877376874	0.11859062979492774	7.808997572439073	0.1187808650343818
7600	167.8608538587849	3.7570591974096295	22.55556862121934	0.23750983458316635	7.554985430624096	0.11449880641056365
7700	178.5583333333333	3.7125070145837147	25.7	1.8498310733685903	7.350747464015723	0.4161140864194907
7800	178.5111111111111	4.873093169336813	20.566666666666666	3.891158068122023	9.356798057010598	1.4253203225315152
7900	188.4472222222222 2	13.989118621800825	25.572222222222223	1.586604807384253	8.180937652348732	0.8152876463370696
8000	197.9666666666666 7	5.3463383107818006	30.936111111111114	1.1845162319291802	6.883343984297379	0.15497174225374544
8100	210.24	4.156970050409302	28.400000000000002	0.5919459434779497	7.817355717235821	0.32259526373448333
8200	221.6333333333333 3	3.503388835589538	26.626666666666665	0.4826316746063566 4	8.501461030380815	0.1058728185633998
8300	224.5499999999999 8	4.171430609914677	29.733333333333334	1.0111874208078362	7.790610016406983	0.15743985738911243
8400	209.2333333333333 5	7.078370810669186	38.73333333333333	0.9291573243177561	5.402003099223259	0.138073845
8500	222.0666666666667	7.702164198024698	38.73333333333333	0.3055050463303911 6	5.733576780875495	0.2088949711057831 4
8600	234.6666666666666 6	8.228203530135438	39.16666666666666 4	1.171893055416463	5.993957838576247	0.2410427869935608 8
8700	245.4666666666666 7	8.673138609138752	39.5	1.1135528725660062	6.213637422695482	0.06957354
8800	254.6833333333333	9.425276300105647	38.43333333333333	0.8504900548115354	6.626301689848617	0.1447589860870814 3

8900	261.1833333333334	9.778846216877204	38.68333333333333	1.0128343069492336	6.750834419323465	0.088873473
9000	266.15	8.858188302356213	37.98333333333333	0.825126253	7.010224760792734	0.30390220935283657
9100	266.45	8.334116629853456	39.28333333333333	0.9169696468985933	6.789637084622963	0.10105997785518947
9200	266.3166666666666	7.130275824	38.59444444444444	0.33085887111061696	6.904944013011584	0.23939708920886915
9300	265.9283333333334	5.9140644512325995	39.33166666666667	0.6587930884073835	6.764227897	0.058017336
9400	268.1914814814815	3.948412766477911	38.87444444444444	0.31755042372029546	6.902166905843598	0.045142513
9500	272.4041512345679	5.0966279542698345	38.729486673185306	0.27948188525974726	6.846595606734177	0.10591191989140353

LETTER OF PAPER SUBMISSION AT JIEE

Pulchowk Campus
Institute of Engineering
Tribhuvan University

NABIN ADHIKARI <078msmde009.nabin@pcampus.edu.np>

[JIEE] Submission Acknowledgement

postmaster@nepjol.info <postmaster@nepjol.info> Thu, May 7, 2026 at 9:38 AM
Reply-To: "Dr. Khem Gyanwali" <gyanwalikhem@ioe.edu.np>
To: Nabin Adhikari <078msmde009.nabin@pcampus.edu.np>

Nabin Adhikari:

Thank you for submitting the manuscript, "Experimental Study of Propellers with Dimpled surface and Serrated Trailing-Edge Geometry" to Journal of Innovations in Engineering Education. With the online journal management system that we are using, you will be able to track its progress through the editorial process by logging in to the journal web site:

Manuscript URL: https://www.nepjol.info/index.php/jiee/authorDashboard/submission/94007
Username: nabinadhikari009

If you have any questions, please contact me. Thank you for considering this journal as a venue for your work.

Dr. Khem Gyanwali

Journal of Innovations in Engineering Education

SIMILARITY REPORT

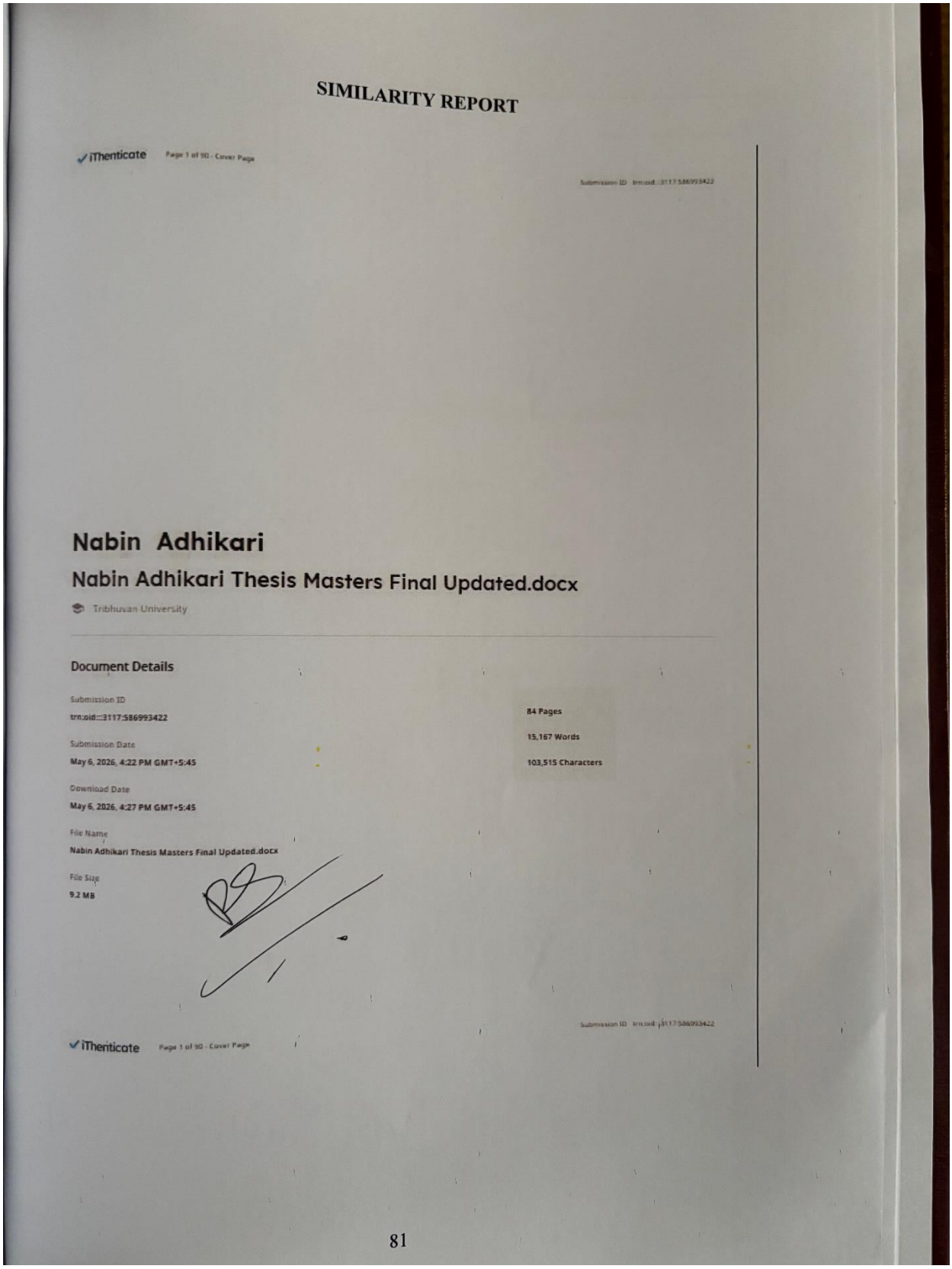

SIMILARITY REPORT

iThenticate Page 1 of 90 - Cover Page

Submission ID trn:oid:::3117:586993422

Nabin Adhikari

Nabin Adhikari Thesis Masters Final Updated.docx

Tribhuvan University

Document Details

Submission ID
trn:oid:::3117:586993422

Submission Date
May 6, 2026, 4:22 PM GMT+5:45

Download Date
May 6, 2026, 4:27 PM GMT+5:45

File Name
Nabin Adhikari Thesis Masters Final Updated.docx

File Size
9.2 MB

84 Pages

15,167 Words

103,515 Characters

Submission ID trn:oid:::3117:586993422

iThenticate Page 1 of 90 - Cover Page

81

11% Overall Similarity

The combined total of all matches, including overlapping sources, for each database.

Filtered from the Report

- Bibliography
- Quoted Text
- Cited Text
- Small Matches (less than 8 words)

Custom Section Exclusions

(titlesCount) Section Titles, (keywordsCount) Keywords

Section title	No. of Section Starters	Section Starters
"Acknowledgements"	4	Acknowledgements, Acknowledgement, Acknowledgment, Acknowledgments

Match Groups

- 81 Not Cited or Quoted 11%
  Matches with neither in-text citation nor quotation marks
- 0 Missing Quotations 0%
  Matches that are still very similar to source material
- 0 Missing Citation 0%
  Matches that have quotation marks, but no in-text citation
- 0 Cited and Quoted 0%
  Matches with in-text citation present, but no quotation marks

Top Sources

- 9% Internet sources
- 5% Publications
- 0% Submitted works (Student Papers)

Integrity Flags

1 Integrity Flag for Review

Hidden Text
9 suspect characters on 8 pages
Text is altered to blend into the white background of the document.

Our system's algorithms look deeply at a document for any inconsistencies that would set it apart from a normal submission. If we notice something strange, we flag it for you to review.

A Flag is not necessarily an indicator of a problem. However, we'd recommend you focus your attention there for further review.

Submission ID trn:oid:::3117:586993422
iThenticate Page 2 of 90 - Integrity Overview

82

Match Groups

- 81 Not Cited or Quoted 11%
  Matches with neither in-text citation nor quotation marks
- 0 Missing Quotations 0%
  Matches that are still very similar to source material
- 0 Missing Citation 0%
  Matches that have quotation marks, but no in-text citation
- 0 Cited and Quoted 0%
  Matches with in-text citation present, but no quotation marks

Top Sources

9% Internet sources
5% Publications
0% Submitted works (Student Papers)

Top Sources

The sources with the highest number of matches within the submission. Overlapping sources will not be displayed.

1	Internet	
elibrary.tucl.edu.np		2%
2	Internet	
www.geeker.co.nz		<1%
3	Internet	
www.researchgate.net		<1%
4	Internet	
www.electronicsforu.com		<1%
5	Internet	
www.coursehero.com		<1%
6	Internet	
www.anyload.com		<1%
7	Internet	
arxiv.org		<1%
8	Internet	
www2.mdpi.com		<1%
9	Publication	
Yijuan Gu, Fuqiang Song, Honglei Bai, Jianing Wu, Kun Liu, Bowen Nie, Liangquan ...		<1%
10	Publication	
Paolo Candeloro, Daniele Ragni, Tiziano Pagliaroli. "Experimental investigation o...		<1%

iThenticate Page 3 of 90 - Integrity Overview Submission ID trn:oid:::3117:586993422

11	Internet	
en.wikipedia-on-ipfs.org		<1%
12	Internet	
graphsearch.epfl.ch		<1%
13	Internet	
iaeme.com		<1%
14	Publication	
Susan Buys, Victoria Oakley. "The Conservation and Restoration of Ceramics", Ro...		<1%
15	Internet	
www.theinfolist.com		<1%
16	Internet	
etd.uum.edu.my		<1%
17	Internet	
researchrepository.ru.ac.za		<1%
18	Internet	
etd.cput.ac.za		<1%
19	Internet	
hdl.handle.net		<1%
20	Internet	
uk.anycubic.com		<1%
21	Publication	
Abdul Qader Abdullah, Sharul Sham Dol. "Aerodynamic Investigation and Design ...		<1%
22	Internet	
etd.aau.edu.et		<1%
23	Publication	
Jenna E. Stolzman, Sanjivan Manoharan. "Testing the Efficacy of Dimples on a NA...		<1%
24	Internet	
en.wikipedia.org		<1%

25	Publication	Pfab, Jonas. "Deciphering Protein Complex Structures from Cryo-Electron Microsc... <1%
26	Internet	www.accessengineeringlibrary.com <1%
27	Publication	A. Larsen, G. L. Larose, F. M. Livesey. "Wind Engineering into the 21st Century - Pr... <1%
28	Publication	Stanewsky, E.. "Adaptive wing and flow control technology", Progress in Aerospac... <1%
29	Internet	www.dti.or.th <1%
30	Internet	www.mdpi.com <1%
31	Publication	A. Arockia Bazil Raj. " FPGA-Based Embedded System Developer's Guide", C... <1%
32	Publication	K. V. Sambasivarao, Anasuya Sesha Roopa Devi Bhima. "Artificial Intelligence, Co... <1%
33	Publication	Pichitkul, Auraluck. "A Unified Approach for Modeling Fluid-Structure Interaction... <1%
34	Publication	Wisniewski, Nathan. "Development of a Cowling With Cooling Ports for Co-Axial P... <1%
35	Internet	dl.astfe.org <1%
36	Internet	dr.ur.ac.rw <1%
37	Internet	erepository.uonbi.ac.ke:8080 <1%
38	Internet	files01.core.ac.uk <1%

39 Internet
irbackend.kiu.ac.ug <1%

40 Internet
iris.cnr.it <1%

41 Internet
sear.unisq.edu.au <1%

42 Internet
soar.wichita.edu <1%

43 Internet
thesis.lib.ncku.edu.tw <1%

iThenticate Page 6 of 90 - Integrity Overview Submission ID trn:oid:::3117:586993422